



Plasma-driven catalytic process for plastic waste upcycling over perovskite-type pre-catalysts

Xiao Yu^a, Aasir Rashid^b, Guoxing Chen^{a,b,*}, Marc Widenmeyer^b, Ulrike Kunz^b,
Tao Shao^c, Gert Homm^a, Leopoldo Molina-Luna^b, Rony Snyders^{d,e}, Anke Weidenkaff^{a,b}

^a Fraunhofer Research Institution for Materials Recycling and Resource Strategies IWKS, Brentanostraße 2a, 63755 Alzenau, Germany

^b Department of Materials and Earth Sciences, Technical University of Darmstadt, Peter-Grünberg-Str. 2, 64287 Darmstadt, Germany

^c Beijing International S&T Cooperation Base for Plasma Science and Energy Conversion, Institute of Electrical Engineering, Chinese Academy of Sciences, Beijing 100190, China

^d Chimie des Interactions Plasma-Surface, University of Mons, 20 Place du Parc, 7000 Mons, Belgium

^e Matera Nova Research Center, 3 Avnuue Copernic, 7000 Mons, Belgium

ARTICLE INFO

Keywords:

Plasma pyrolysis

Perovskite-type pre-catalyst

Plastic waste upcycling

H₂

Metal oxide-carbon composite materials

ABSTRACT

The increasing demand for plastics poses significant challenges for post-consumer waste management. In this work, we propose a novel plasma-thermal catalytic tandem process over perovskite-type La_{0.6}Ca_{0.4}Co_{1-x}Fe_xO_{3-δ} (LCCF) pre-catalysts for upcycling plastic waste into H₂ and value-added metal oxide-carbon composite materials. Among the evaluated pre-catalysts, La_{0.6}Ca_{0.4}Co_{0.2}Fe_{0.8}O_{3-δ} prepared by ultrasonic spray synthesis (USS) demonstrated the highest performance, achieving an H₂ yield of 54.7 mmol/g_{plastic} (~76.6 % of theoretical H₂ production) with a selectivity of 78 %. Morphological differences between pre-catalysts synthesized via USS and co-precipitation appear to play a crucial role in their catalytic efficiency. Life cycle assessment results indicate that the ultrasonic spray synthesis method is more environmentally sustainable than the co-precipitation method for LCCF production. Considering the high H₂ yield during plastic upcycling using the La_{0.6}Ca_{0.4}Co_{0.2}Fe_{0.8}O_{3-δ} pre-catalyst prepared by USS, along with its lower environmental impact during pre-catalyst production compared to the co-precipitation method, the plasma-thermal catalytic tandem process using this pre-catalyst offers a promising and sustainable approach to plastic waste upcycling.

1. Introduction

In 2022, the global production of plastics exceeded 400 million metric tonnes (Mt), of which only 8.9 % came from recycling processes, with the majority still derived from fossil sources [1]. Addressing the defossilization challenge of the chemical industry and the environmental issues caused by non-degradable post-consumer plastic waste necessitate a robust waste management strategy.

Among the various methods for processing plastic waste, mechanical recycling is often preferred due to its simplicity. This approach enables waste to be reprocessed into new products, though often with degraded properties [2]. However, it requires uncontaminated and sorted waste streams [3]. When segregation is unfeasible, incineration [4] is widely used to recover the energy from the plastic waste. The process is associated with significant greenhouse gas emissions and the potential production of toxic gases or hazardous by-products, leading to obvious

environmental disadvantages. Thermochemical technologies such as solvolysis, gasification, and pyrolysis [5] offer promising alternatives for recovering valuable chemicals (e.g. monomers, monomer precursors and other chemical substances) from waste [6], providing solutions for handling non-recyclable, mixed or heavily contaminated plastic waste streams [7]. Plasma gasification has been extensively studied for solid waste treatment due to its ability to convert plastic wastes into H₂-rich syngas without emitting harmful by-products [8–11]. However, the high capital and operational costs, along with its energy-intensive nature, limit the economic feasibility of this process [12]. Pyrolysis is another widely studied method within the circular economy framework for plastics [13]. It involves a thermochemical decomposition process that occurs at temperatures ranging from 350–800 °C under an inert atmosphere, with or without the presence of a catalyst [14]. This process enables the generation of various valuable chemical products such as gas, oil, wax and solid residues [15–18]. The presence of a suitable

* Corresponding author at: Department of Materials and Earth Sciences, Technical University of Darmstadt, Peter-Grünberg-Str. 2, 64287 Darmstadt, Germany.
E-mail address: guoxing.chen@mr.tu-darmstadt.de (G. Chen).

<https://doi.org/10.1016/j.cej.2025.161954>

Received 22 November 2024; Received in revised form 21 March 2025; Accepted 23 March 2025

Available online 1 April 2025

1385-8947/© 2025 The Author(s). Published by Elsevier B.V. This is an open access article under the CC BY-NC license (<http://creativecommons.org/licenses/by-nc/4.0/>).

catalyst can further tailor the product distribution to favour the desired products. The co-production of hydrogen and carbon materials is of significant interest, as it enables hydrogen production alongside carbon capture and storage, managing the simultaneous plastic waste upcycling and energy recovery in a potentially sustainable manner.

Various processes have been explored to achieve this, with one of the most extensively studied methods being the two-stage catalytic thermal process (as illustrated in Fig. S1). Plastic wastes are initially pyrolyzed at temperatures above 500 °C at the first-stage to produce hydrocarbon gases [19–23]. These gases are then processed in the so-called catalytic stage to reform hydrogen and facilitate the growth of carbon nano-materials. Despite its advantages, this method often generates a significant amount of undesirable oil by-products, thereby reducing its overall efficiency. Additionally, the process achieves only acceptable product yields after long reaction time, which results in huge energy consumption. To address these issues, improvements such as the incorporation of a Dielectric Barrier Discharge (DBD) non-thermal plasma in the second stage (as shown in Fig. S2) has been explored to improve the H₂ production as well as to lower the operating temperature for the catalytic process from e.g., 800 °C to 250 °C [24,25], consequently reducing the energy consumption. However, the decreasing temperature is not owing to the change of reaction mechanism under the existence of a plasma environment. The temperature of 250 °C for the DBD reactor was chosen to avoid rapid condensation of the pyrolysis hydrocarbons in the plasma-catalyst reactor. And due to this lower temperature, no carbon nano-materials can be generated. Microwave-initiated catalytic pyrolysis (as shown in Fig. S3) has been considered as a promising chemical upcycling method for converting plastics into hydrogen and carbon nanomaterials at high production yields within short reaction times [26–28]. However, the success of this method critically depends on the application of suitable heat susceptors, which are supposed to be evenly distributed within the plastic feedstock for energy delivery. Besides, this process generally requests a large catalyst consumption to ensure satisfactory production yields [27–30]. Direct contact between catalysts and plastics can lead to catalyst deactivation due to the poisoning from plastic additives, which poses challenges for continuous plastic decomposition. Both of these issues negatively impact the economic efficiency of this method and restrict its feasibility especially for scaling to industrial applications.

Each mentioned pyrolysis method possesses their own advantages and disadvantages. Combining multiple approaches can help maximize their benefits while minimizing drawbacks, ensuring high recycling efficiency along with economic and energy viability, particularly for large-scale pyrolysis. To achieve this, we proposed a plasma-enabled process for rapid upcycling of plastics in our previous work [31], which can rapidly decompose various plastics into hydrogen and carbon materials within seconds with reasonable product yields without the presence of catalysts. The yields and the quality of generated carbon materials can be further promoted by introducing catalysts in the integrated thermal catalytic process. Moreover, since in the plasma-enabled process, the catalysts are not required to be mixed with plastic streams and serve as heat subsectors like that in a microwave-imitated process [26,32,33]. The integrated thermal catalytic process provides mild and controllable reaction conditions and enables more possibilities for catalyst selection. Low cost, easy synthesis, sustainable catalysts with good catalytic performance are the key factors for further enhance the efficiency of the process from a circular economic aspect and enable industry-scale application. It is important to note that carbon accumulation on the catalyst surface leads to gradual deactivation, and separating carbon nanotubes from the catalyst remains a significant challenge that should be carefully considered. If the resulting metal oxide–carbon composite materials can be directly utilized without requiring separation, the high catalyst volume would be less critical in case of large-scale application. Studies have shown that metal oxide–carbon nanotube composites have potential applications as electrocatalysts and in energy storage systems, such as batteries [34–36] and solid oxide cells (SOCs) [37]. For these

applications, catalyst selection plays a crucial role. The use of perovskite-type materials for plastic waste pyrolysis offers a promising approach, enabling H₂ production alongside potential metal-oxide–carbon composite materials for energy storage applications. Introducing perovskite-type pre-catalysts into the plasma-thermal catalytic tandem process could provide a promising strategy for plastic waste upcycling, an area that remains largely unexplored. Further improvements, such as developing more environmentally friendly catalyst synthesis methods, will be essential to enhancing the sustainability of this process.

In this study, we explored a plasma-thermal catalytic tandem process with the introduction of perovskite-type La_{0.6}Ca_{0.4}Co_{1-x}Fe_xO_{3-δ} (x = 0.5, 0.8) pre-catalysts for sustainable plastic waste upcycling. To further reduce environmental impact and enhance catalytic performance, we systematically compared catalysts prepared via co-precipitation (CP) synthesis and the newly introduced ultrasonic spray synthesis (USS). The physicochemical properties of the pre-catalysts and the resulting carbon materials were thoroughly characterized using state-of-the-art analytical techniques. Life cycle assessment (LCA) was also applied to investigate the environmental impacts (EI) associated with the two employed synthesis techniques. The findings of this work may provide valuable insights into a promising strategy for sustainable plastic waste management.

2. Experimental section

2.1. Pre-catalyst preparation

The perovskite-type La_{0.6}Ca_{0.4}Co_{1-x}Fe_xO_{3-δ} (x = 0.5, 0.8) pre-catalysts, namely La_{0.6}Ca_{0.4}Co_{0.5}Fe_{0.5}O_{3-δ} (LCCF6455) and La_{0.6}Ca_{0.4}Co_{0.2}Fe_{0.8}O_{3-δ} (LCCF6428) were prepared by the following two methods [38–40]:

Co-precipitation (CP) method: Weighed solution of metal nitrates—La(NO₃)₃·6H₂O (Alfa Aesar, 99.9 %), Ca(NO₃)₂·4H₂O (Sigma-Aldrich, >99 %), Co(NO₃)₂·6H₂O (Sigma-Aldrich, >98 %), and Fe(NO₃)₃·9H₂O (Sigma-Aldrich, >98 %)—was slowly added to an ammonium carbonate solution under vigorous stirring at a temperature of 60 °C. The pH of the mixture was adjusted to 8.5–9 using ammonium carbonate (Alfa Aesar) to form a precipitate suspension. The precipitates were aged at 60 °C for 1 h with continuous stirring, followed by filtration and multiple washes with hot demineralized water to remove excess ions. The prepared material was dried at 110 °C for 12 h, then crushed and calcined in air at 1050 °C for 5 h to obtain the final pre-catalysts powder.

Ultrasonic spray synthesis (USS) method: Weighed quantities of metal nitrates were dissolved in deionized water to prepare the precursor solution (0.05 mol in 50 mL). This solution was subsequently introduced into the nebulizing chamber of an ultrasonic spray synthesis (USS) apparatus (see Fig. S4). A thin transparent foil was used to separate the solution from the ultrasonic nebulizer, which generated ultrasonic waves to convert the precursor solution into fine droplets. An inert gas (argon) flow at 2000 sccm was used to transport the aerosolized droplets into a heated tube furnace maintained at 900 °C. As the aerosol droplets travelled through the furnace, they underwent sequential precipitation and pyrolysis reactions, resulting in the formation of product particles. These particles coalesced to form polycrystalline solid powder. The powder product was collected at a production rate of up to 2.5 g/h and subsequently dried in an oven at 100 °C for 30 min.

To simplify the discussion of the studied perovskite-type pre-catalysts, we have adopted a systematic labelling approach based on elemental composition and the synthesis method. Specifically, La_{0.6}Ca_{0.4}Co_{0.5}Fe_{0.5}O_{3-δ} (LCCF6455) and La_{0.6}Ca_{0.4}Co_{0.2}Fe_{0.8}O_{3-δ} (LCCF6428) synthesized via co-precipitation (CP) method are labelled as LCCF6455-CP and LCCF6428-CP, respectively. Similarly, those synthesized via ultrasonic spray synthesis (USS) method are designated as LCCF6455-USS and LCCF6428-USS, respectively.

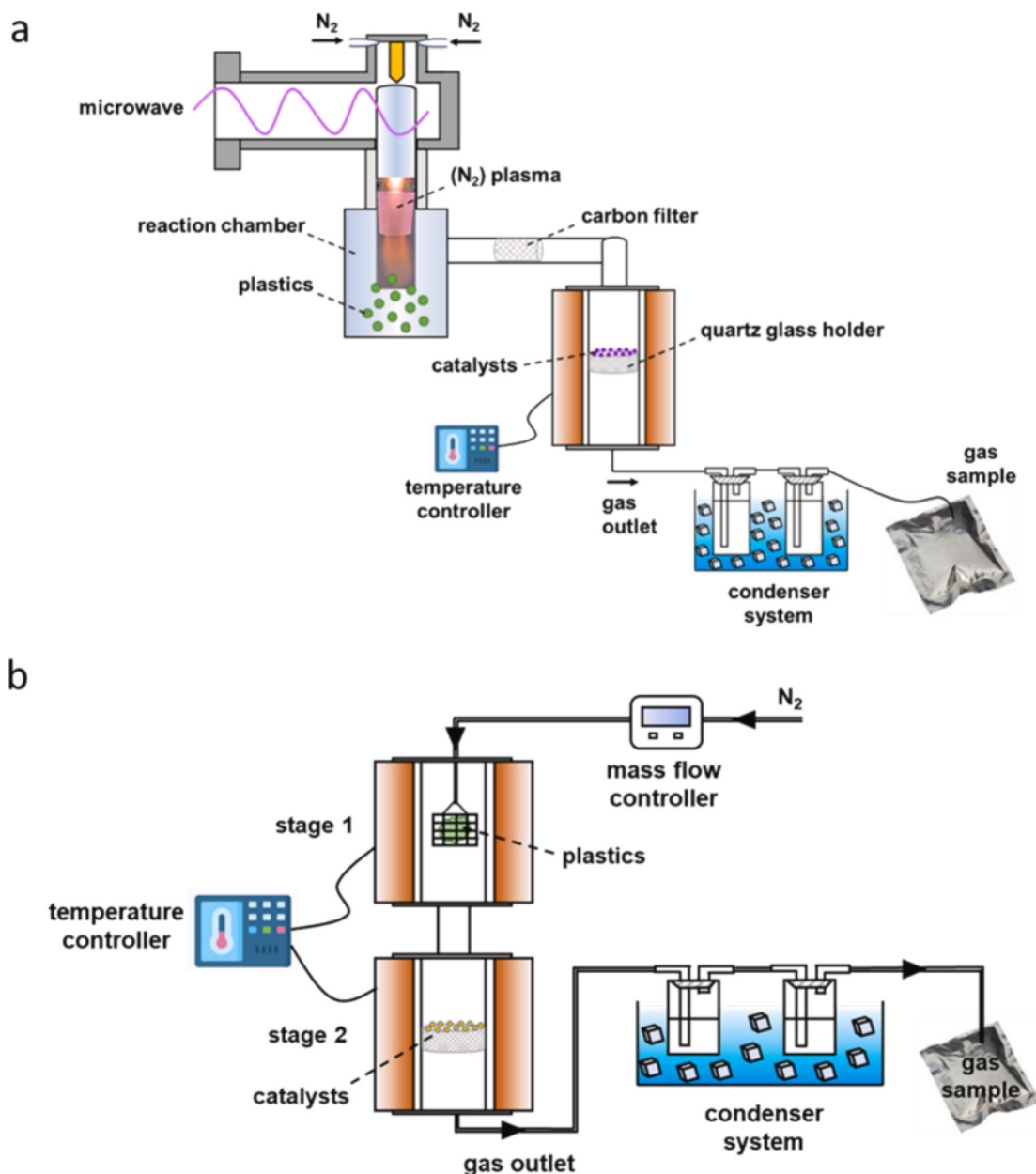


Fig. 1. Schematic diagrams of (a) the plasma-thermal catalytic tandem system and (b) the thermal catalytic pyrolysis system for plastic waste upcycling. The actual temperatures of the catalyst/CNT bed during CNT synthesis were not measured.

2.2. Characterization of materials

The crystal structures of the fresh pre-catalysts were analyzed by Powder X-ray diffraction (XRD) using a PANalytical empyrean X-ray diffractometer ($Co-K\alpha_1$). The diffraction patterns were recorded from 10° to 90° (2 theta) with a scanning rate of $0.5^\circ/\text{min}$. Brunauer-Emmett-Teller (BET) analysis was performed to determine the surface texture information of the fresh pre-catalysts through N_2 adsorption at -196.15°C . The spent samples were measured by a micro-Raman spectrometer (Bruker) with a 532 nm laser as the excitation wavelength at 2 mW for the Raman spectra. A Zeiss-MERLIN scanning electron microscope (SEM) equipped with an OXFORD X-ray detector for Energy-dispersive X-ray spectroscopy (EDXS) was employed for detecting the surface morphology as well as the elemental information at a 15 kV acceleration voltage. High-resolution images and EDXS information were provided by a JEM2100F (JEOL) transmission electron microscope (TEM) equipped with an X-ray detector. Temperature program oxidation

(TPO) measurements were performed with a NETZSCH STA 449F3. The samples were heated at a rate of $10^\circ\text{C}/\text{min}$ from room temperature up to 900°C in an alumina crucible in air with a flow rate of $30\text{ mL}/\text{min}$.

2.3. Experimental setup and experiment procedure

The experiments were conducted using a plasma-thermal catalytic tandem system as shown in Fig. 1(a). It includes a plasma pyrolysis process (first stage) and a thermal catalytic process (second stage). An atmospheric microwave plasma discharge at 2.45 GHz from MUEGGE was used at the first stage to decompose plastic feedstock, which was added into a self-designed reaction chamber before starting the experiments. In this work, discarded low-density polyethylene (LDPE) packing bags and medical FFP1 masks (PP) household wastes were manually cut into approximately 2 mm pieces using a common scissor and used as feedstock without further pre-processing. In literature, $\sim 0.5 - 1\text{ g}$ plastic was typically used in the two-stage thermal catalytic process

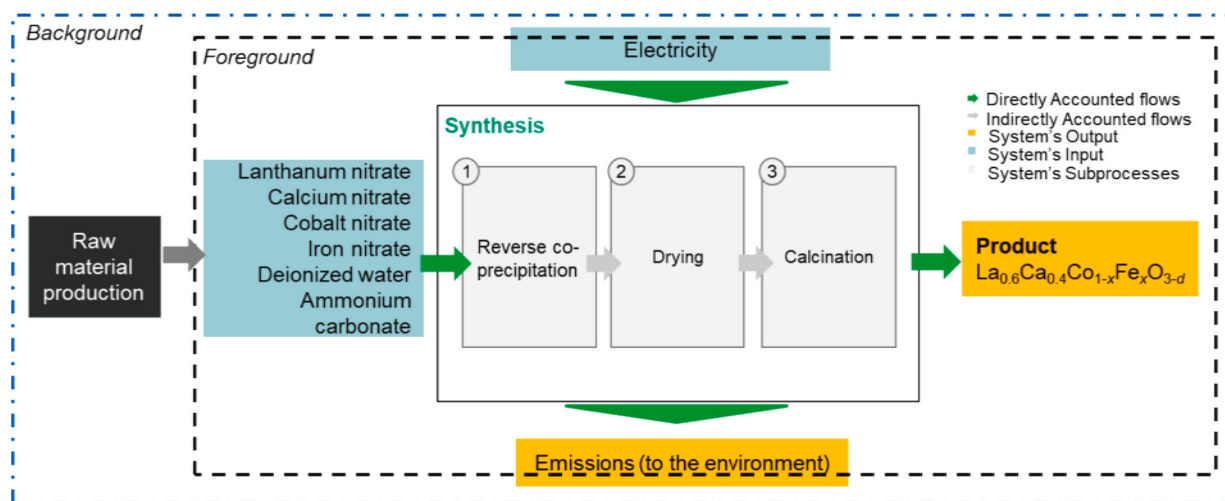


Fig. 2. LCA flowsheet for the synthesis of LCCF using the reverse co-precipitation (CP) method.

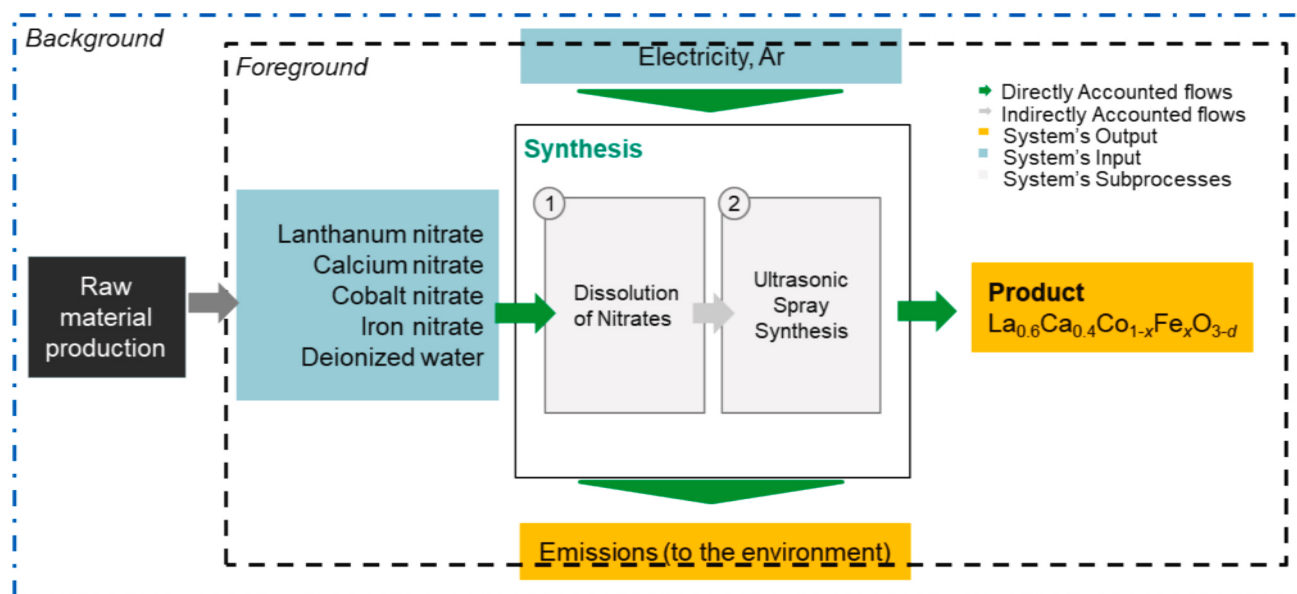


Fig. 3. LCA flowsheet for the synthesis of LCCF using the ultrasonic spray synthesis (USS) method.

[23,41–47] while ~ 0.4 g plastic was used in the microwave-initiated catalytic process [27,29,30,48,49]. To ensure a fair comparison with literature reports, we conducted our experiments in the plasma-enabled system using 0.4 g of plastic. In principle, the system can process over 100 g of plastic using the same powder input and flow rate. However, due to current lab safety regulations, conducting large-scale experiments remains challenging. To address this, we are in the process of installing a 915 MHz microwave plasma system with a 75,000 W capacity in a technical hall, which will be capable of processing hundreds of kilograms of plastic waste per hour once completed.

In the integrated thermal process, 0.4 g of the studied perovskite-type pre-catalysts were placed inside the catalytic reactor. At the start of each experiment, the entire system was purged with N_2 at a flow rate of 5 L/min (regulated by an electronic mass flow controller) for 5 min to remove residual air. Following the purge, the second-stage thermal catalytic process was heated to reach 800 °C. Once this temperature was achieved, plastic pyrolysis was initiated by igniting the microwave plasma, which operated at a power input of 1000 W for 2.5 min to ensure complete decomposition of the feedstock. The resulting gaseous products were collected in a gas sample bag for further analysis. The plasma-

only pyrolysis experiment (without integrating the thermal catalytic process) was conducted under the same reaction conditions using 0.4 g of plastic as a reference.

To fairly compare the performance of our plasma-thermal catalytic process with the conventional two-stage thermal catalytic process, we tried to conduct experiments under similar reaction conditions to better understand the underlying mechanistic differences between the two methods. In our study, some reaction conditions for the two-stage thermal catalytic pyrolysis process (as shown in Fig. 1(b)) were intentionally modified, making them distinct from those typically reported in the literature [45,50–52]. Unlike conventional processes, where plastics are introduced at the beginning of the experiment and gradually decomposed as the temperature increases over a defined period (~ 30 min), our approach was designed to align more closely with the rapid heating characteristics of the plasma process. Specifically, since the plasma process can rapidly reach ~ 800 °C, we introduced plastics into the system only after the first stage of the thermal catalytic pyrolysis process had already reached this temperature. Consequently, the reaction time for plastic decomposition was significantly shorter (~ 2.5 min). The thermal pyrolysis experiments without pre-catalysts were also

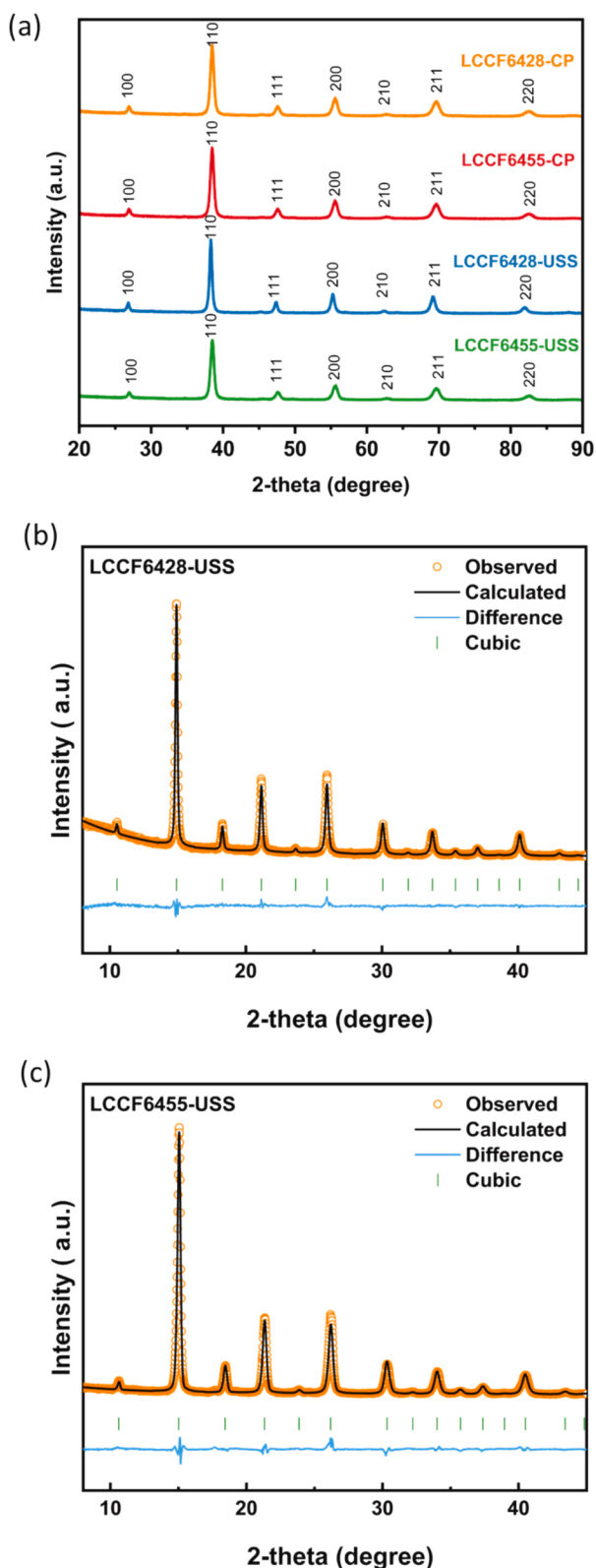


Fig. 4. (a) XRD patterns ($\text{Co-K}\alpha_1$) of fresh $\text{La}_{0.6}\text{Ca}_{0.4}\text{Co}_{0.2}\text{Fe}_{0.8}\text{O}_{3-\delta}$ (LCCF6428) and $\text{La}_{0.6}\text{Ca}_{0.4}\text{Co}_{0.5}\text{Fe}_{0.5}\text{O}_{3-\delta}$ (LCCF6455) pre-catalysts prepared by coprecipitation (CP) and ultrasonic spray synthesis (USS) methods. A pseudo-cubic indexing was used. (b, c) Rietveld refinements of the XRD patterns of fresh $\text{La}_{0.6}\text{Ca}_{0.4}\text{Co}_{0.2}\text{Fe}_{0.8}\text{O}_{3-\delta}$ (LCCF6428) and $\text{La}_{0.6}\text{Ca}_{0.4}\text{Co}_{0.5}\text{Fe}_{0.5}\text{O}_{3-\delta}$ (LCCF6455) pre-catalysts prepared by ultrasonic spray synthesis (USS) method.

performed as the references. To prevent systemic or experimental errors, each experiment was performed three times. The average value was used in the analysis, and the error bars representing the standard deviations of the data are shown on the diagrams.

The collected produced gases were analyzed using an Agilent 7890B gas chromatograph (GC) equipped with a flame ionization detector (FID) and a thermal conductivity detector (TCD). Selectivity (vol%), as defined by GC analysis, is the volume percent of each product component in the generated gases (Eq. (1)). The H_2 yield ($\text{mmol}/\text{g}_{\text{plastic}}$) is defined as the quantity of H_2 (mmol) produced per gram of reactant plastic, outlined in Eq. (2). The H_2 yield (%) in percentage is then calculated by comparing the mass of H_2 generated to the theoretical mass of H_2 that could be produced from the starting plastic, as indicated in Eq. (3). Hydrogen efficiency, or hydrogen atom recovery efficiency, is determined by comparing the total hydrogen mass in all gas products to the theoretical hydrogen content of the starting plastic feedstock (see Eq. (4)). The solid (carbon) yield was determined by the mass fraction of the produced carbon materials relative to the mass of the plastic feedstock (see Eq. (5)), with the mass of the catalysts excluded from the total mass of the produced carbon materials. Eq. (6) defines the gas yield as the corresponding mass fractions in relation to the mass of plastic feedstock. Since in the plasma process, the liquid yield is limited and therefore difficult to measure, it is evaluated from the quantities of measurable solid and gas yields following Eq. (7).

$$\text{Selectivity (vol\%)} = \frac{\text{Volume of specific product component (L)}}{\text{Volume of all the generated gases (L)}} \quad (1)$$

$$\text{H}_2 \text{ yield (mmol/g}_{\text{plastic}}) = \frac{\text{Millimol of H}_2 \text{ produced (mmol)}}{\text{Mass of plastic (g)}} \quad (2)$$

$$\text{H}_2 \text{ yield (\%)} = \frac{\text{Mass of H}_2 \text{ produced (g)}}{\text{Theoretical H}_2 \text{ produced from plastic (g)}} \times 100\% \quad (3)$$

$$\text{Hydrogen efficiency (\%)} = \frac{\sum \text{mass of H atoms contained in gas products (g)}}{\text{Theoretical mass of H atoms in plastic (g)}} \times 100\% \quad (4)$$

$$\text{Solid yield (\%)} = \frac{\text{Mass of produced carbon materials (g)}}{\text{Mass of plastic (g)}} \times 100\% \quad (5)$$

$$\text{Gas yield (\%)} = \frac{\text{Mass of gas produced (g)}}{\text{Mass of plastic (g)}} \times 100\% \quad (6)$$

$$\text{Liquid (oil) yield (\%)} = 100\% - \text{Gas yield} - \text{Solid yield} \quad (7)$$

2.4. Life cycle assessment (LCA) methodology of LCCF pre-catalyst synthesis

A cradle-to-gate attributional life cycle assessment (LCA) was carried out on the studied LCCF pre-catalysts at the laboratory scale. The LCA study followed the standards ISO 14040 [53] and ISO 14044 [54]. The environmental impact (EI) assessment was performed using the ILCD (International Reference Life Cycle Data System) 2011 midpoint + impact assessment method [55], which includes 15 impact indicators covering key categories of human health, availability of resources, and the natural environment. These indicators include acidification, material resources depletion, ozone depletion, human toxicity, climate change, eutrophication, and others. The assessment was conducted using the OpenLCA software (version 1.10.3) with background data requirements met by the ecoinvent database (version 3.9.1). Figs. 2 and 3 represent the LCA flowsheets for the two synthesis methods used.

The goal of this assessment was to study and compare the environmental impact (EI) associated with both synthesis techniques to determine the method that produces LCCF with a lower EI at different

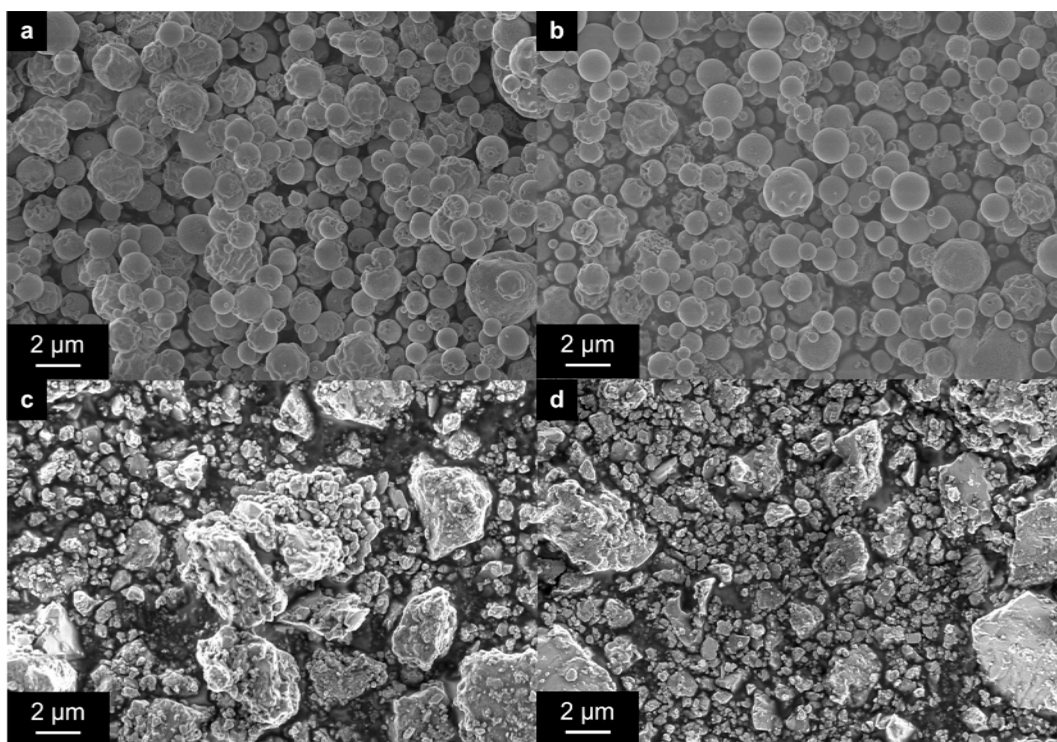


Fig. 5. SEM images of the fresh pre-catalysts: (a) LCCF6455-USS, (b) LCCF6428-USS, (c) LCCF6455-CP, (d) LCCF6428-CP.

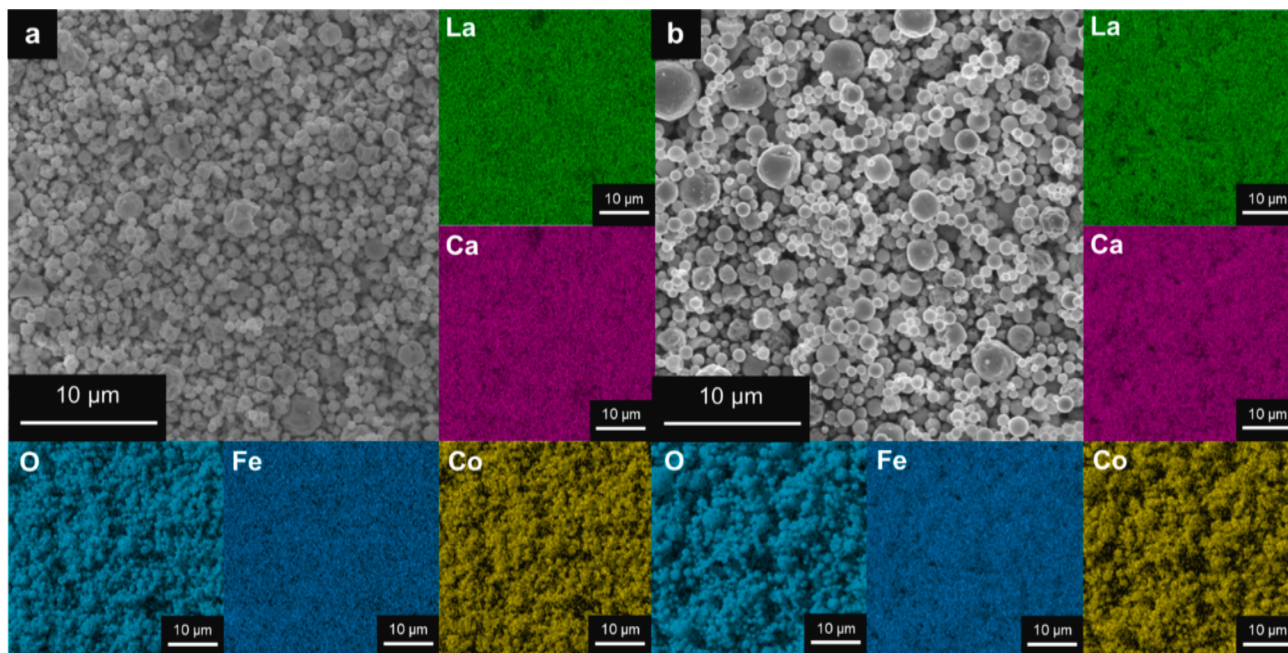


Fig. 6. SEM-EDXS analysis of fresh catalysts: (a) LCCF6455-USS, (b) LCCF6428-USS.

production scales. Two functional units of 1 kg and 1 g were designed and investigated. The main reasons behind selecting two functional units are largely due to the difference in the mode of synthesis and the sources of energy consumption in the two synthesis techniques. As shown in Fig. 14, in the co-precipitation (CP) method, the drying and calcination process can be done with a box furnace. Since the furnace can easily accommodate 1 kg of the sample at once, the energy consumption for the preparation process is basically the same whether 1 kg or 1 g sample is prepared. In contrast, the ultrasonic spray synthesis

(USS) shown in Fig. 15 utilizes a direct production path. Here, a precursor solution of metal nitrates dissolved in deionized water is converted to precursor-containing droplets through nebulization. These droplets are transported as an aerosol by a carrier gas (argon) into a preheated tube furnace, where they undergo repeated precipitation and subsequently pyrolysis, forming polycrystalline powder products [39,56]. No additional calcination step is needed. The energy consumption in this process primarily depends on the run time of the tube furnace acted by the power of the nebulizer. The current setup uses a 30

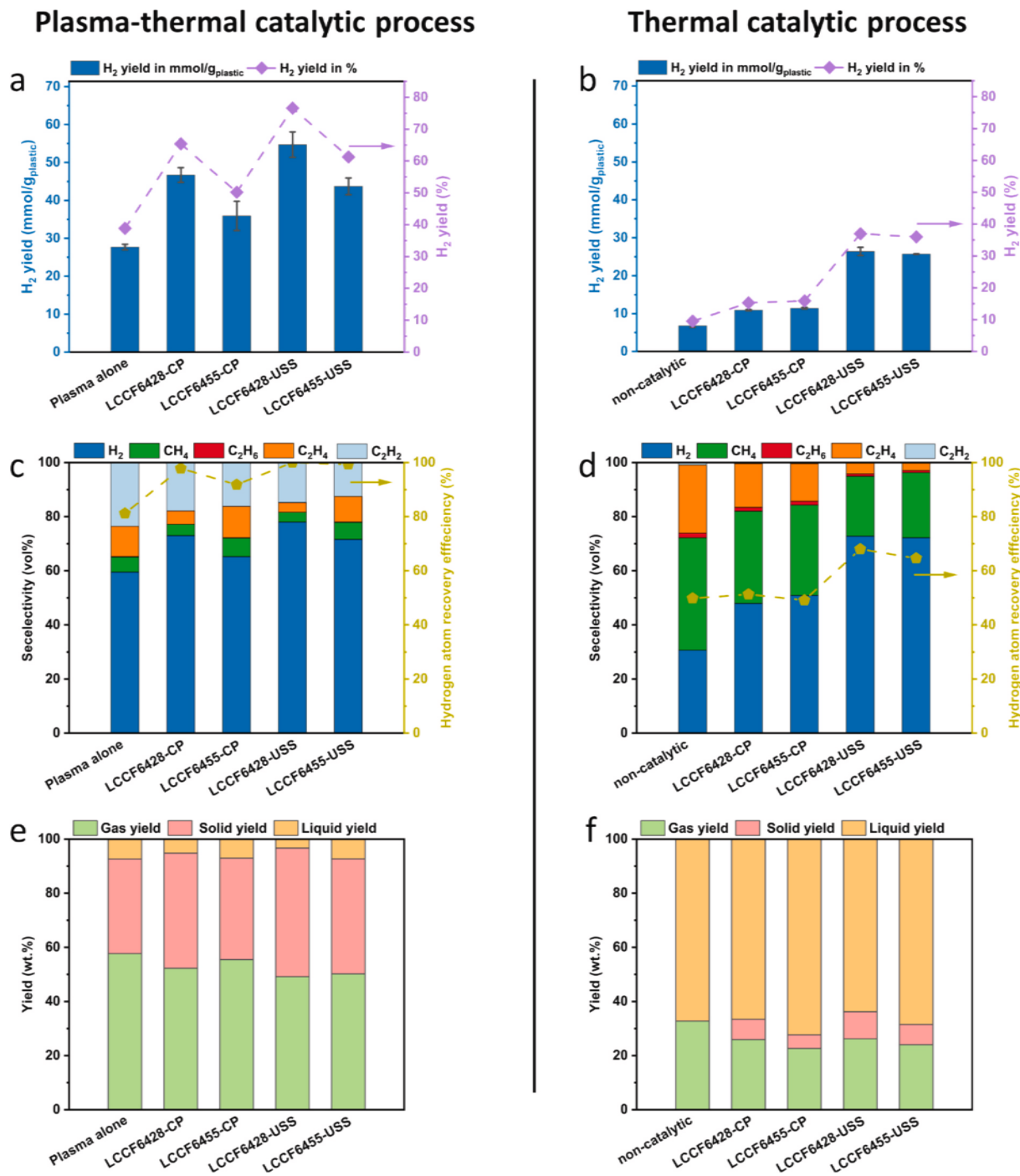


Fig. 7. (a, b) H₂ yield (mmol/g_{plastic} and %), (c, d) selectivity in the evolved gases (vol%) and hydrogen atom recovery efficiency (%), and (e, f) product yields (wt.%) in the plasma-thermal catalytic tandem process and two-stage thermal catalytic process over studied LCCF pre-catalysts. A non-catalytic plasma alone experiment and a non-catalytic two-stage thermal pyrolysis experiment were performed as references. For a single test, 0.4 g of pre-catalyst and 0.4 g of discarded shopping bags (LDPE) were employed.

W nebulizer generating ultrasonic waves at 1.7 MHz leading to a production rate of ca. 2.5 g per hour (g/h) of LCCF. Applying a linear upscaling scenario, the production rate can be increased to 50 g/h using a commercially available 600 W nebulizer without affecting the tube furnace's energy consumption. In this study, the 30 W nebulizer was used for the preparation of 1 g of LCCF-USS, and the utilization of the 600 W nebulizer was assumed for the preparation of 1 kg of LCCF-USS. Detailed information about the life cycle inventory can be assessed from the [supporting information](#) (Table S1–S4).

3. Results and discussion

3.1. Characterization of as-prepared $\text{La}_{0.6}\text{Ca}_{0.4}\text{Co}_{1-x}\text{Fe}_x\text{O}_{3-\delta}$ pre-catalysts

Fig. 4(a) presents the XRD patterns of fresh $\text{La}_{0.6}\text{Ca}_{0.4}\text{Co}_{0.2}\text{Fe}_{0.8}\text{O}_{3-\delta}$ (LCCF6428) and $\text{La}_{0.6}\text{Ca}_{0.4}\text{Co}_{0.5}\text{Fe}_{0.5}\text{O}_{3-\delta}$ (LCCF6455) pre-catalysts prepared by co-precipitation (CP) and ultrasonic spray synthesis (USS) methods. The patterns confirm that all pre-catalysts exhibit characteristic perovskite-type phase reflections with pseudo-cubic indexing [39],

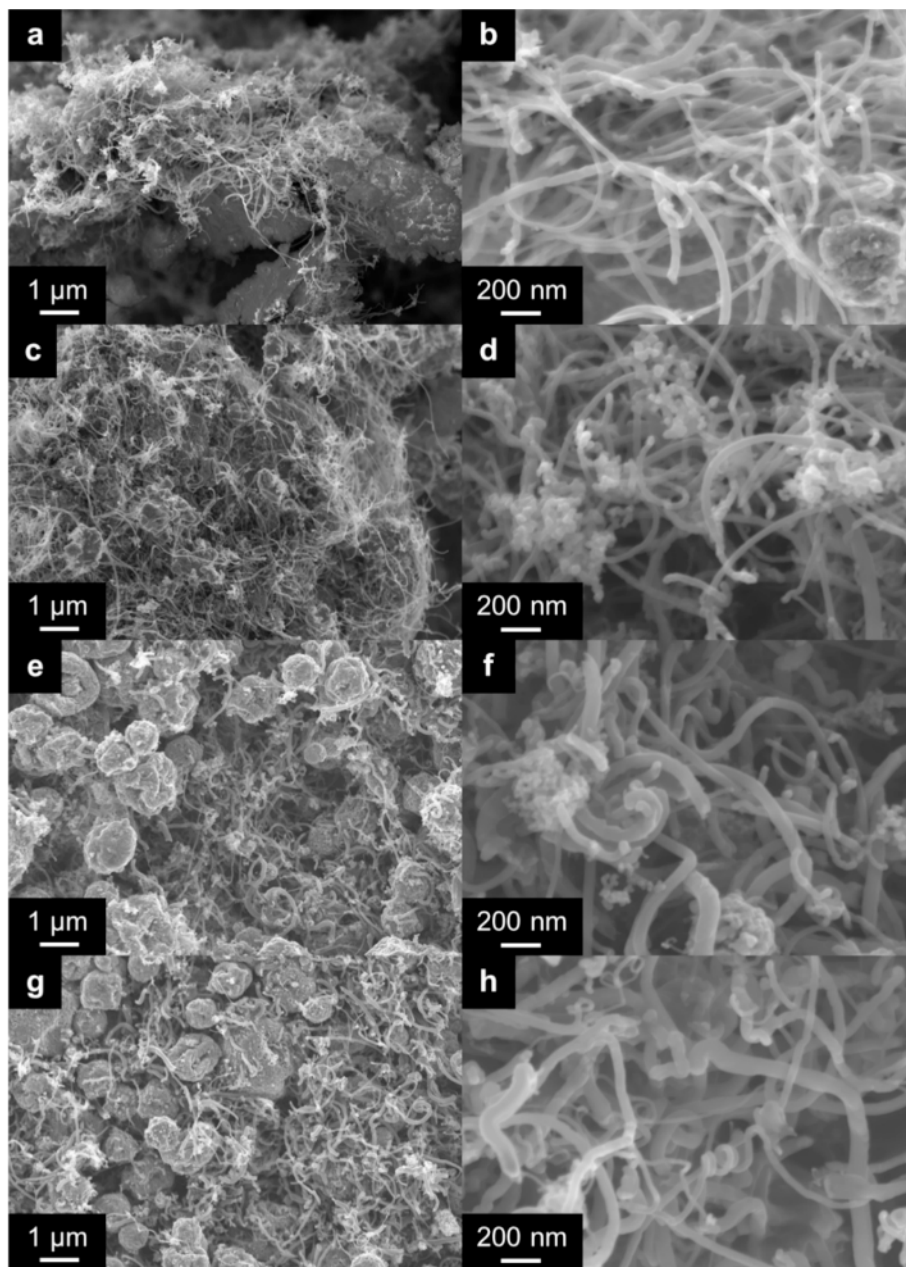


Fig. 8. SEM images of generated carbon materials over LCCF catalysts from plasma-thermal catalytic process: (a,b) LCCF6455-CP; (c,d) LCCF6428-CP, (e,f) LCCF6455-USS, (g,h) LCCF6428-USS.

devoid of any impurities. No difference can be found between the patterns of catalysts with different composition, it suggests that variations in the Co/Fe ratio do not induce major changes in the crystal structure. Detailed structural information of catalysts prepared through USS method can be observed by Rietveld refinements of XRD patterns. As shown in Fig. 4(b) and Fig. 4(c), the collected diffraction data of both LCCF6428-USS and LCCF6455-USS are perfectly fitted by a perovskite-type phase. Fig. 5 and Fig. S5 show the SEM images of the fresh LCCF6455 and LCCF6428 pre-catalysts prepared using the USS and CP methods. The LCCF-USS pre-catalyst samples display sphere-like particles, while the LCCF-CP samples appear as irregular, bulk-like particles. These observations are consistent with the results of the LCCF-CP samples reported in our previous study [23]. The Co/Fe ratio appears to have a limited effect on the morphology. As shown in Table S5, all samples exhibit very low specific surface areas. Variations in morphology do not appear to significantly influence the porosity or

surface area of the investigated pre-catalysts. The EDXS analysis shown in Fig. 6 and Fig. S6 indicate a uniform distribution of Ca, La, Co, Fe, and O elements on the surface of the pre-catalysts prepared by both the USS and CP methods.

3.2. Plasma-thermal catalytic tandem process for plastic waste upcycling over perovskite-type pre-catalysts and comparison with two-stage thermal catalytic pyrolysis

In this study, the plasma-thermal catalytic tandem process using perovskite-type pre-catalysts for upcycling discarded packaging bags (LDPE) and medical masks (PP) from everyday waste was investigated. A series of conventional two-stage thermal catalytic processes were conducted under similar reaction conditions to enable a fair comparison and to better understand the mechanism differences between the two methods. The results, including H₂ yield, gas selectivity, hydrogen atom

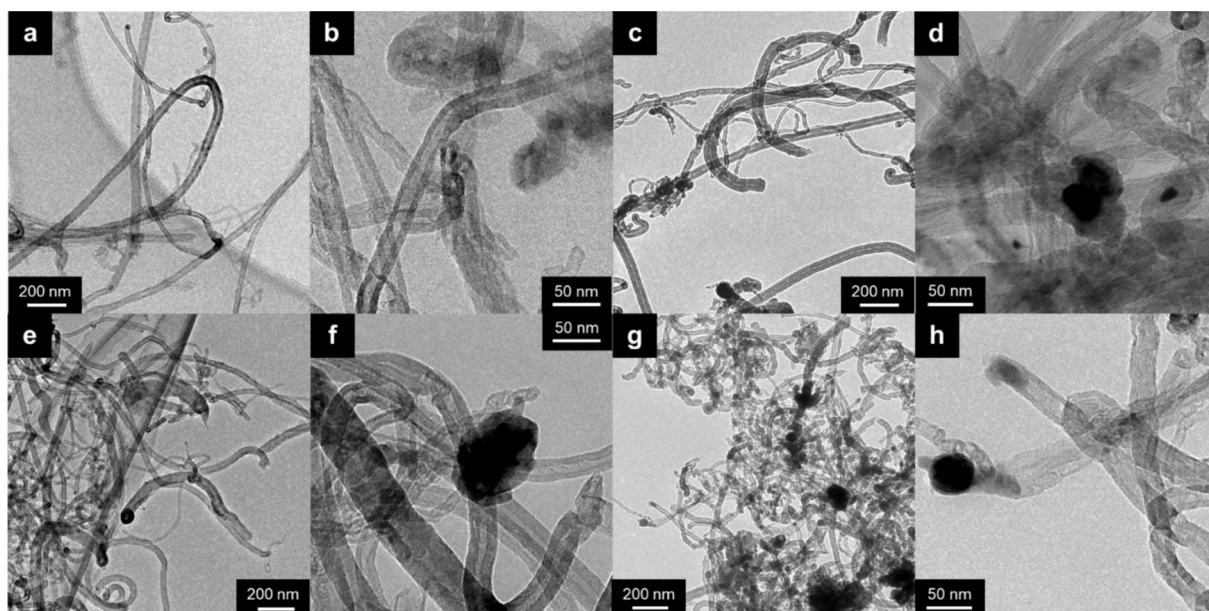


Fig. 9. TEM images of the carbon materials produced over LCCF pre-catalysts in the plasma-thermal catalytic process: (a, b) LCCF6455-CP; (c, d) LCCF6428-CP; (e, f) LCCF6455-USS; (g, h) LCCF6428-USS.

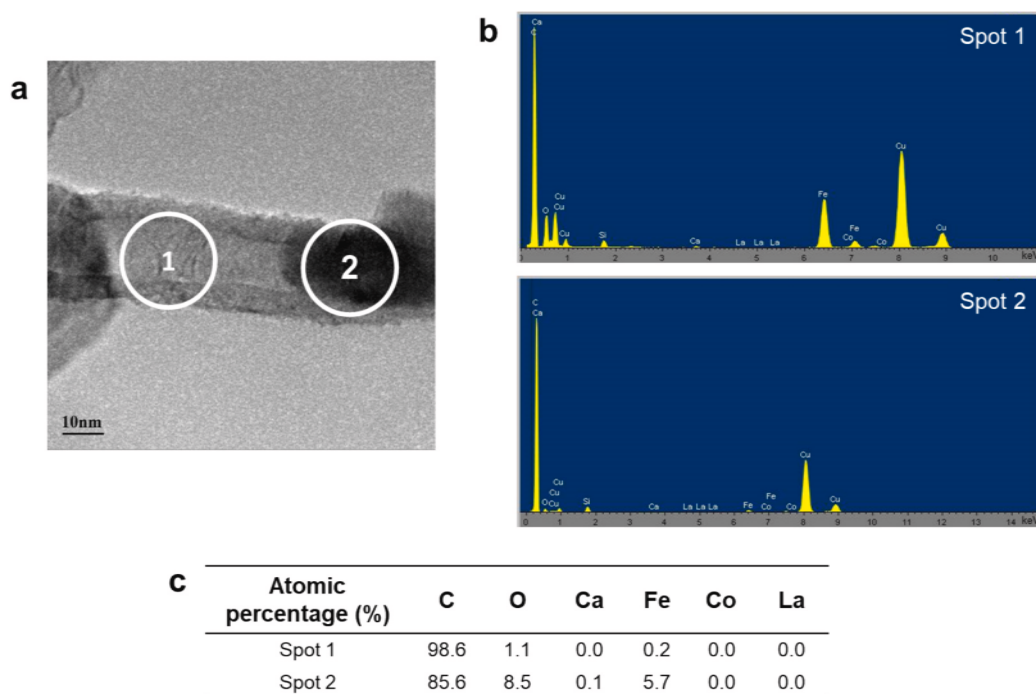


Fig. 10. TEM images with EDXS spectra of the carbon materials produced over the LCCF6428-USS pre-catalyst in the plasma-thermal catalytic process. The detected Cu is from the copper grid. (a) TEM image of LCCF6428-USS, (b) element distribution analysis of the selected spots and (c) atomic percentage of different elements at selected spots.

recovery efficiency, and product yields, are presented in Fig. 7. Overall, the plasma-thermal catalytic tandem process delivers satisfactory transformation yields of both gaseous and solid products across the studied catalysts. Less than 10 % liquid product yields are overserved in all the cases. Regarding the production of H_2 , it is clear that introducing the perovskite-type pre-catalysts to the integrated thermal catalytic process can improve the H_2 yield as well as the selectivity comparing with the plasma alone process. An over 60 % H_2 selectivity can be achieved in all the plasma-thermal catalytic tandem process. The pre-catalysts synthesized by the ultrasonic spray synthesis method (LCCF-

USS) generally indicate better catalytic performance in producing H_2 than the pre-catalysts prepared by the co-precipitation method (LCCF-CP). The elemental composition of catalysts also affects their catalytic activity. A lower Co/Fe ratio in the pre-catalysts (LCCF6428) can result in increased H_2 generation and higher H_2 selectivity, which aligns with the findings in our previous research [23]. Additionally, this composition reduces the usage of critical cobalt [57] during the catalyst synthesis in comparison to pre-catalysts with a higher Co/Fe ratio, making it a more resource-efficient option. Across all the investigated pre-catalysts, LCCF6428-USS provides the highest H_2 selectivity of 78 %

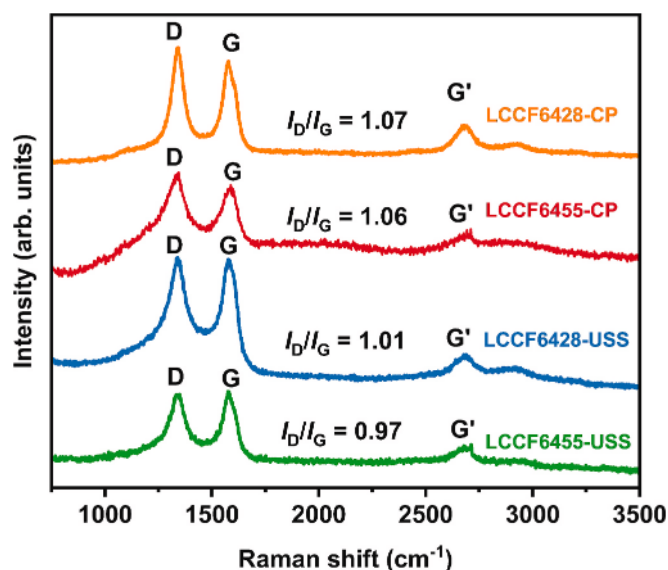


Fig. 11. Raman analysis of carbon materials produced over LCCF pre-catalysts in the plasma-thermal catalytic process.

and the H_2 yield of $54.7 \text{ mmol/g}_{\text{plastic}}$, which is almost doubled as for the plasma alone process ($27.7 \text{ mmol/g}_{\text{plastic}}$).

In the thermal pyrolysis process without the presence of the pre-catalysts, a significantly lower H_2 yield of $6.8 \text{ mmol/g}_{\text{plastic}}$ is

obtained, which is only around 1/4 of that in the plasma alone non-catalytic process. The achieved H_2 selectivity is only 30.1%. Although employing the studied LCCF pre-catalysts can obviously improve both the yield and selectivity of H_2 , the highest yield achieved ($26.4 \text{ mmol/g}_{\text{plastic}}$) with the LCCF6428-USS pre-catalyst is still much lower than that of plasma alone pyrolysis. Based on these findings, we propose that the high H_2 yield achieved in the plasma-thermal catalytic process is driven by chemical pathways induced by plasma, extending beyond simple thermal decomposition. In plasma, energetic reactive species, including electrons, radicals, ions, excited species, and photons, collide intensely with polymer molecules once the plasma is initiated. Within seconds, sufficient energy is delivered to break C-H and C-C bonds, facilitating the rapid decomposition of the polymer. Plasma efficiently breaks chemical bonds in plastics, promoting the fragmentation of larger C_xH_y molecules. Additionally, the presence of a highly active catalyst enhances H_2 production by facilitating the dehydrogenation of C_2H_2 during the thermal catalytic process.

3.3. Carbon materials production over $La_{0.6}Ca_{0.4}Co_xFe_{1-x}O_{3-\delta}$ pre-catalysts

To study the morphology of solid products produced from discarded packing bags (LDPE) in the plasma-thermal catalytic process, the spent pre-catalysts with generated (carbon) materials were collected and observed using SEM and TEM. Crowded and dense elongated fibrous filamentous carbon materials with smooth surfaces, as shown in Fig. 8, were found by SEM in all investigated cases of plasma-thermal catalytic

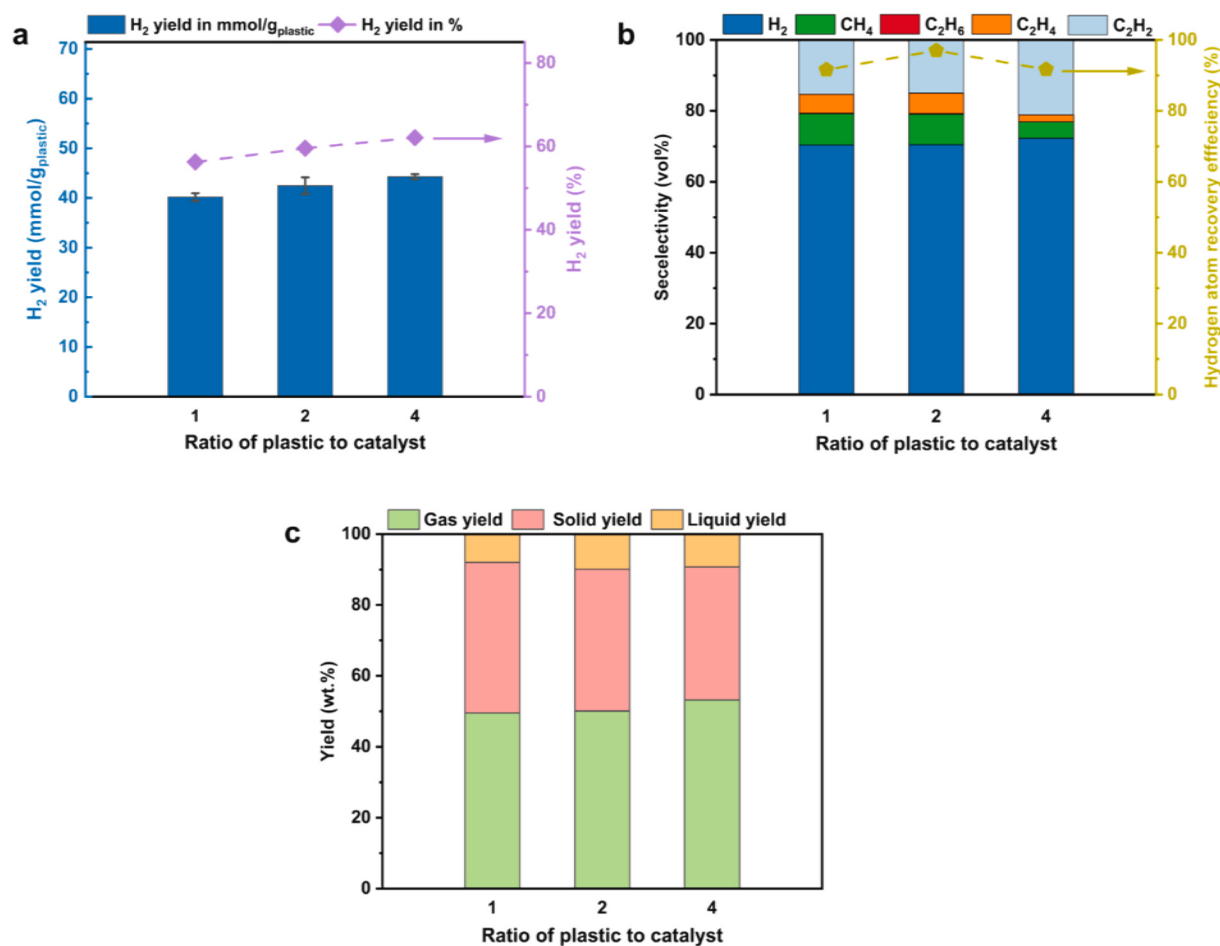


Fig. 12. (a) H_2 yield ($\text{mmol/g}_{\text{plastic}}$ and %), (b) gaseous product composition (vol%) and hydrogen atom recovery efficiency (%), and (c) product yields (wt.%) of plasma-thermal catalytic tandem process over LCCF6428-USS pre-catalyst with different ratios of plastic to pre-catalyst. For a single test, 0.4 g of discarded FFP1 medical masks (PP) was employed as the feedstock.

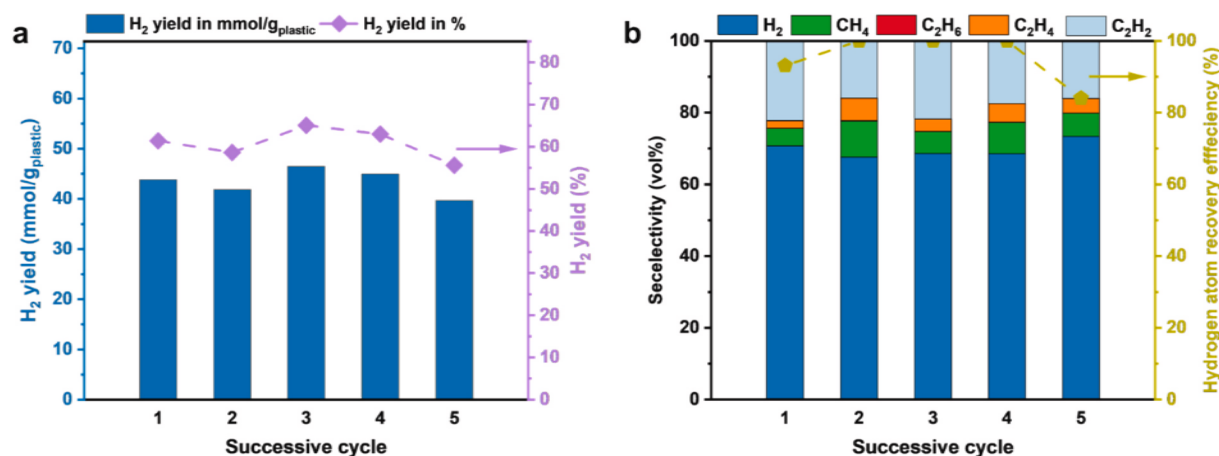


Fig. 13. Successive cycles of the decomposition of discarded FFP1 medical masks (PP) in the plasma-thermal catalytic pyrolysis over LCCF6428-USS pre-catalyst with a plastic-to-pre-catalyst ratio of 4. (a) H₂ yield (mmol/g_{plastic} and %) and (b) gaseous product composition (vol%) and hydrogen atom recovery efficiency (%). In each cycle, 0.4 g of plastic is used as feedstock, and the pre-catalyst is 0.1 g throughout the entire cyclic measurement without further addition.

process. In the two-stage thermal catalytic process, the carbon nano-materials formed using the same pre-catalysts displayed a bamboo-like structure [58–60], where the walls are periodically partitioned like bamboo stalks, characterized by short lengths and rough surfaces (see Fig. S7). The differences become evident when observed with TEM, as shown in Fig. 9 and Fig. S8. It is also noteworthy that the valuable carbon materials can be generated in the plasma-only process, as shown in Fig. S9. However, no clear evidence indicates a relationship between the morphology of the formed carbon materials and the corresponding pre-catalysts employed. In addition to surface morphology, the TEM images in Fig. 9 also reveal that the filamentous carbon products generated in the plasma-thermal catalytic tandem process exhibit clear hollow structures, suggesting that they are more likely to be nanotubes rather than nanofibers. The observed nanotube-like carbon materials generated from discarded packing bags have outer diameters in the range of around 10–40 nm. The most acceptable mechanism for the growth of carbon nanotubes follows a three-step process [61]. Initially, carbon species decomposed from hydrocarbons on the surface of catalyst particles, which subsequently diffuse on the particles' surface or through the particles as a solid solution. In the final step, the carbon atoms precipitate to form nanotubes [61,62]. As observed in the TEM-EDXS analysis in Fig. 10, Fig. S10, and Table S6, Co and Fe are reduced in situ from the La_{0.6}Ca_{0.4}Co_xFe_{1-x}O_{3-δ} pre-catalysts, and these reduced species could serve as the active sites for the decomposition of carbon-containing precursors. XRD analysis with La_{0.6}Ca_{0.4}Co_{1-x}Fe_xO_{3-δ} samples after the plasma-thermal catalytic pyrolysis of plastic experiments were conducted and the results are shown in Fig. S11. All samples underwent a certain degree of reduction due to the generated H₂, while their perovskite structure was largely preserved. These findings suggest that, in the plasma-thermal catalytic process, Co and Fe species exsolved from the perovskite-type pre-catalysts likely act as active clusters for nanocarbon formation. Notably, when apply Co₃O₄ and Fe₂O₃ were used alone as catalysts under identical conditions, carbon nanotube formation was not observed, as confirmed by the SEM images of the spent samples (see Fig. S12). These results indicate that Co and Fe species are generated in situ from the pre-catalysts while maintaining the perovskite structure, serving as active sites for capturing carbon species and facilitating carbon nanotube formation. The results of temperature programmed oxidation (TPO) further confirmed the generated carbon species. As shown in Fig. S13, the derivative weight changes of the spent pre-catalysts with deposited solid products at 550–600 °C indicate the presence of carbon nanotube-like materials [63–65].

Raman spectroscopy was also used to analyze the produced carbon materials in order to assess the purity and microstructural information of carbon nanomaterial (see Fig. 9). A Raman spectrum with three sharp

bands can be identified in all investigated samples (see Fig. 11). The sharp band at 1350 cm⁻¹ (D band) is attributed to amorphous or disordered carbon and refers to a breathing mode of hexagonally arranged carbon atoms (A_{1g} symmetry), such as in graphene- and graphite-related carbons [66]. The G band at 1580 cm⁻¹ is created by an in-plane mode (E_{2g} symmetry) of carbon atoms (indicating a graphite carbon structure), whereas the G' band at 2700 cm⁻¹ is owing to the second-order two-phonon scattering process and an overtone of the D band [67–69]. The intensity ratio of the D and G band I_D/I_G is utilized to estimate the degree of disorder in the carbon deposits. The I_D/I_G values shown in Fig. 9 indicate a similar disorder degree can be achieved when applying different investigated catalysts to produce carbon nano-materials. These results illustrate that the investigated plasma-thermal catalytic process can successfully produce high-value added carbon nanomaterials by decomposing the daily-life plastic wastes. It may open a new avenue for sustainable plastic waste management.

3.4. Effect of ratios of feedstock plastic and pre-catalyst

Based on the above results, the La_{0.6}Ca_{0.4}Co_{0.2}Fe_{0.8}O_{3-δ} synthesized through the ultrasonic spray method (LCCF6428-USS) demonstrated the best catalytic performance for promoting the plastic decomposition in the plasma-thermal catalytic pyrolysis process. It was chosen as the representative pre-catalyst to further optimize the process. Several studies have indicated that the ratio of feedstock plastic to applied catalysts can significantly influence H₂ yield, gaseous product composition, and overall product yields. These factors can vary considerably when different catalysts are used [28–30,48,70]. Therefore, a series of experiments were conducted using the LCCF6428-USS pre-catalyst to investigate the relationship between the plastic-to-catalyst ratio and the decomposition outcomes. Experiments were performed with three different ratios (1, 2, and 4), and the corresponding results are presented in Fig. 12. Overall, the plastic-to-catalyst ratio had a limited effect on H₂ yield and selectivity. Reducing catalyst consumption can provide economic benefits, particularly when scaling the process to an industrial level. For the studied LCCF6428-USS pre-catalyst, the plastic-to-catalyst ratio was modified to 4. It can provide an H₂ yield of 44.3 mmol/g_{plastic} at a selectivity of 72.3 % when decomposing 0.4 g plastic feedstocks.

3.5. Successive cycle of plastics waste decomposition in the plasma-enabled thermal (plasma-thermal) pyrolysis process

Compared to the thermal catalytic process and plasma alone process, the plasma-thermal catalytic process as a tandem technology can obviously enhance the conversion of plastic wastes to H₂ and valuable

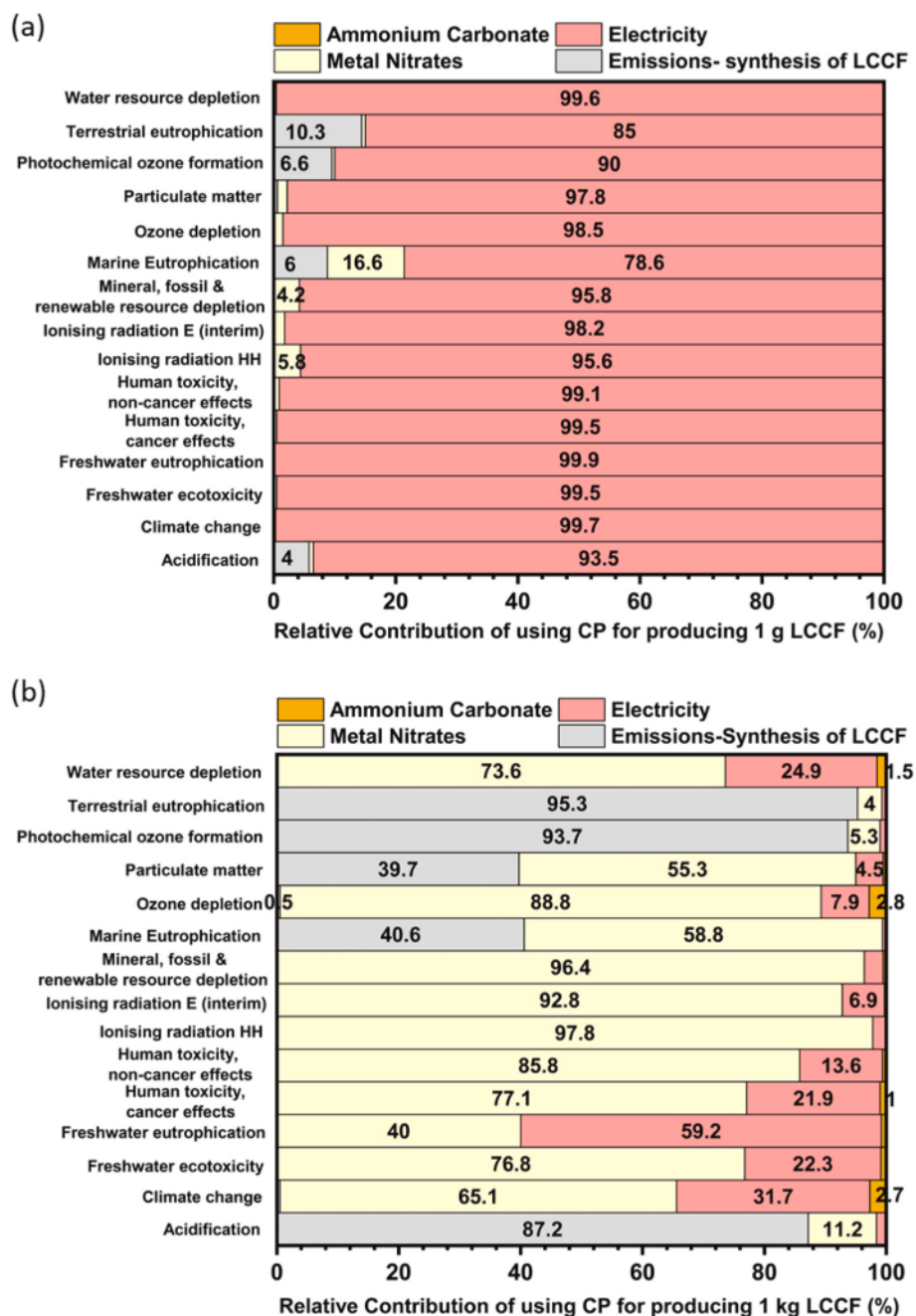


Fig. 14. Comparison of detailed contributions of involved flows towards relevant impact indicators for the environmental impact (EI) in the preparation of (a) 1 g and (b) 1 kg LCCF using the CP method. The units for the relevant indicators shown in the figure are provided in Table S7.

carbon nanomaterials. To further investigate the deactivation behaviour and the operation stability of the pre-catalyst, a series of cycle measurements were performed using the LCCF6428-USS pre-catalyst with a modified plastic-to-pre-catalyst ratio of 4 according to previous results from this work. Discarded FFP1 medical masks (PP) weighing 0.4 g were employed as the feedstock plastics, fed into the system for each cycle without the addition of fresh pre-catalysts. To maintain consistent experimental conditions, the pre-catalyst was not collected until the end of the cycle measurements. Five cycles were successfully performed under defined conditions, with the results for H₂ yield and selectivity of different gaseous products shown in Fig. 13.

Overall, the H₂ yield remained relatively stable around 40 mmol/g_{plastic}, with selectivity maintaining approximately 70 % throughout the cyclic measurements. No significant changes in H₂ production or gaseous product composition were observed, indicating that pre-catalyst

deactivation was minimal. This stability can be attributed to the plasma-thermal catalytic tandem process, where catalysts are employed in the integrated thermal catalytic process. In this setup, the catalysts are primarily exposed to gases generated from the plasma pyrolysis of plastic waste, rather than directly interacting with the solid plastics. This minimizes catalyst deactivation and poisoning from additives in the plastic feedstocks. As a result, a high H₂ yield of 39.7 mmol/g_{plastic} was achieved even after five test cycles, with the highest yield of 46.5 mmol/g_{plastic} (equivalent to 65.1 % of the theoretical H₂ production) reached during the third cycle.

3.6. Life cycle assessment (LCA) of LCCF pre-catalyst synthesis

To further compare and understand the environmental impact resulting from the different synthesis methods of pre-catalysts, an LCA

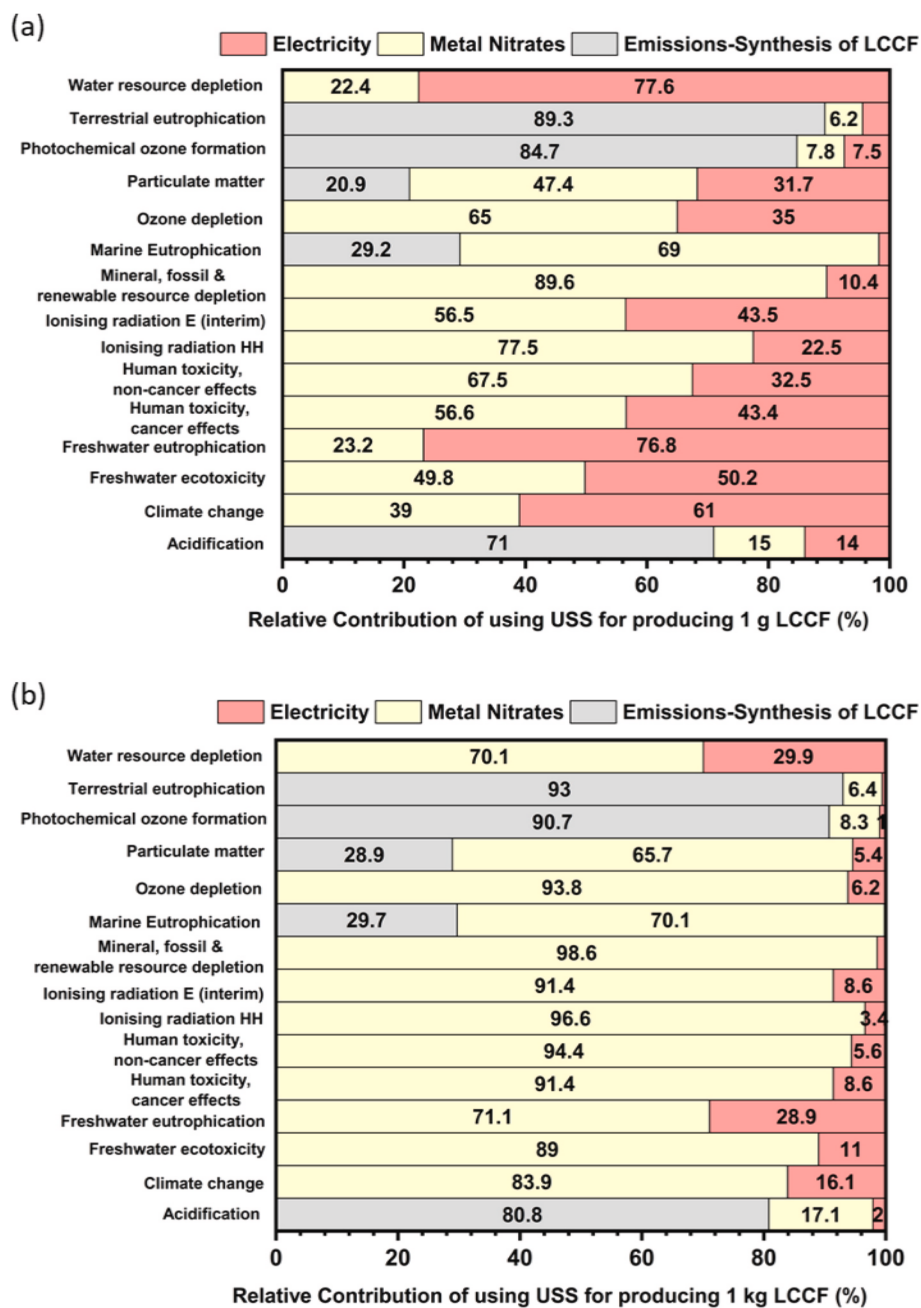


Fig. 15. Comparison of detailed contributions of involved flows towards relevant impact indicators for the environmental impact (EI) in the preparation of (a) 1 g and (b) 1 kg LCCF using the USS method. The units for the relevant indicators shown in the figure are provided in Table S7.

was carried out. For the production of 1 g of LCCF using the CP method, as shown in Fig. 14(a), it is clear that electricity consumption predominates the EI in all impact indicators. Metal nitrates seem to affect marine eutrophication and ionising radiation, while direct process emissions primarily impact terrestrial and marine eutrophication. The EI from ammonium carbonate is limited in all impact indicators and can be neglected. Upscaling the production to 1 kg shifts the EI burden from mainly electricity consumption to metal nitrates, as shown in Fig. 14(b), due to the similar energy consumption as for the production of 1 g. Metal nitrates (especially lanthanum nitrate and cobalt nitrate) used in larger-scale synthesis have a significant EI in most impact indicators, particularly in human health and toxicity, with relative contributions over 96%. Additionally, direct process emissions (NO_x , CO_2 , and H_2O) heavily impact terrestrial eutrophication, photochemical ozone formation and acidification, with contributions over 87%. Compared to the synthesis

process for 1 g of LCCF catalyst, the impact of ammonium carbonate in the synthesis of 1 kg increases in most impact indicators but remains at a limited level.

For the production of 1 g of LCCF using the USS method, as shown in Fig. 15(a), the EI profile differs from the CP method. While energy consumption dominates in all impact factors for CP, metal nitrates have a competitive contribution in 8 of the 15 impact indicators for USS. In resource depletion and marine eutrophication, metal nitrates show significantly higher contributions compared to energy consumption. The EI of direct process emissions (NO_x and H_2O) produced during the synthesis is dominant in terrestrial eutrophication, photochemical ozone formation, and acidification, contributing over 70%. For the simulated 1 kg upscaled LCCF production using USS method, similar to using CP, the large consumption of metal nitrates significantly increases their contribution towards most impact indicators, as shown in Fig. 15(b).

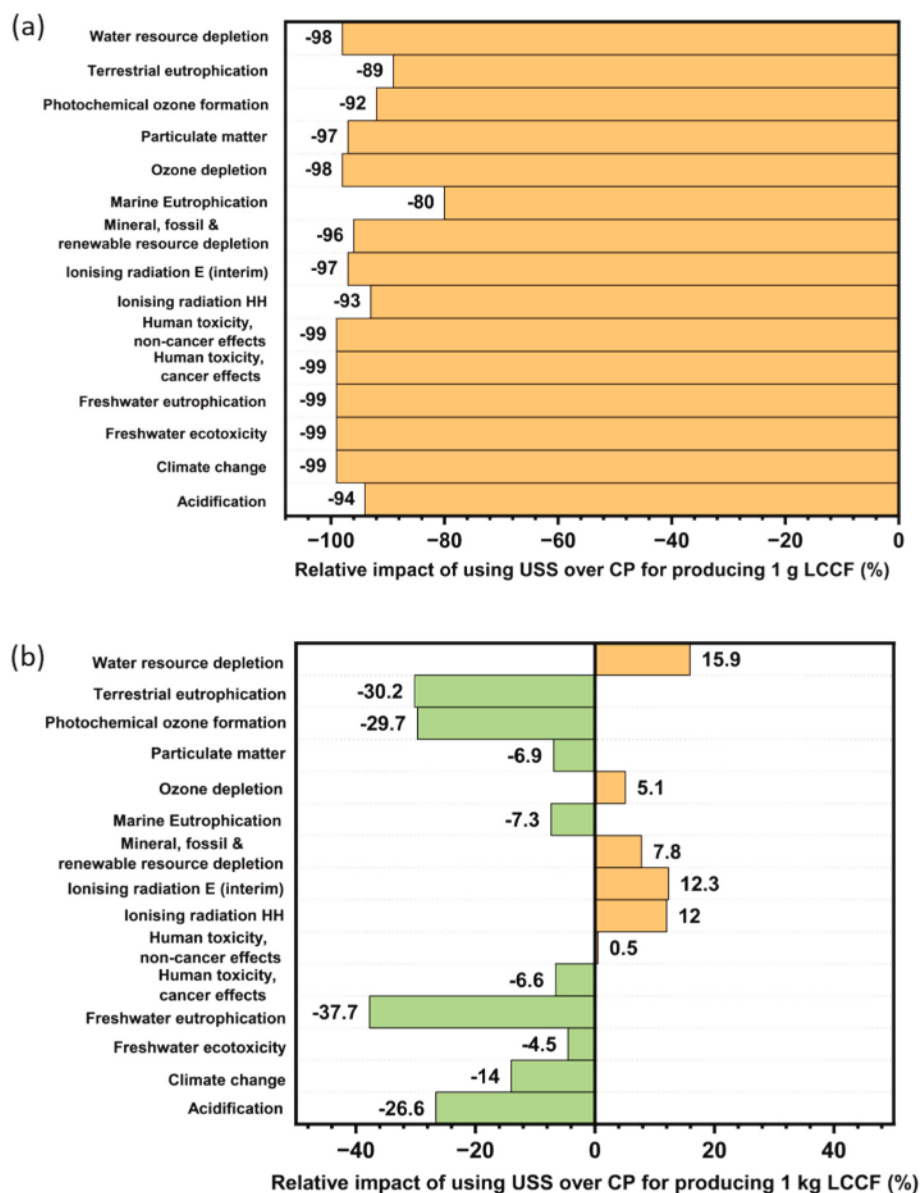


Fig. 16. Comparison of environmental impact (EI) and relevant impact indicators between USS method and CP method for the production of (a) 1 g and (b) 1 kg LCCF pre-catalysts. The units for the relevant indicators shown in the figure are provided in Table S7.

This shift makes metal nitrates as the primary contributors instead of electricity consumption in several impact indicators, such as water resource depletion and freshwater eutrophication, when compared to the smaller-scale synthesis of 1 g. Additionally, process emissions remain dominant in terrestrial eutrophication, photochemical ozone formation, and acidification for the upscaled production.

To sum up, the employed synthesis method (CP or USS) and the scale of synthesis (1 g or 1 kg) both have significant effects on the major impact indicators contributing to the environmental impact (EI) and the corresponding relative contributions. To gain a clear impression of how EI is influenced by the synthesis method, a comparison between USS and CP methods at synthesis scale of 1 g and 1 kg is further performed, as shown in Fig. 16, Table S7 and Table S8.

At the 1 g scale, a decrease in EI across all impact indicators can be observed, with an average decrease of 93 % for LCCF synthesized with USS method. A maximum decrease of 99 % is seen in several impacts such as climate change, freshwater, resource depletion, and human toxicity (see Fig. 16(a)). This is due to significantly lower energy requirements and lower overall direct process emissions of the USS

method compared to CP method. The comparison of 1 kg production of LCCF through two methods indicates a decrease in EI in 9 of the 15 impact indicators when using USS method (see Fig. 16(b)). The EI of LCCF production towards climate change is reduced by 14 % when using USS. This decrease can be attributed to the sole use deionized water as the solvent in USS, thereby avoiding direct CO₂ emissions. In contrast, ammonium carbonate used in the CP method serves as a source of CO₂ emissions. Additionally, overall NO_x emissions are lower in the USS method as shown in Table S1–S4, leading to a decrease in freshwater eutrophication, terrestrial eutrophication, marine eutrophication, photochemical ozone formation, and acidification by an average of 25 %. However, due to approximately 11 % higher lanthanum nitrate consumption in USS compared to CP (as shown in Table S2 and Table S4), resource depletion has increased by around 8 %. An increase in ozone depletion and ionizing radiation can be observed as well.

This LCA study provides a detailed comparative environmental assessment of CP and USS synthesis methods for LCCF pre-catalysts. It identifies key contributors to EI at different scales, demonstrating the advantages of USS in reducing energy consumption and emissions. The

Table 1
Comparison of H₂ yield, selectivity and energy yield (gH₂/kWh) with representative literature.

Process	Catalyst	Type of plastic	Temperature (°C)	H ₂ yield (mmol/g _{plastic})	H ₂ Selectivity (vol %)	Energy yield (gH ₂ /kWh)	Ref.
Plasma pyrolysis	–	LDPE	800	27.7	24.7	0.532	This
Plasma-thermal catalytic tandem process	LCCF6428-USS	LDPE	800	54.7	78.0	0.144	work
	LCCF6455-USS			43.7	65.2	0.115	
	LCCF6428-CP			46.7	78.0	0.123	
	LCCF6455-CP			35.9	71.6	0.094	
Microwave –initiated catalytic process	FeAlO _x	PP	300–380	50.2	73.7	0.361	[26]
	FeAlO _x	PS		23.1	76.1	0.166	
	FeAlO _x	HDPE		55.6	41.6	0.4	
	Fe ₂ O ₃			19.1	61.3	0.138	
	Fe ₃ O ₄			29.7	69.5	0.214	
	Co ₃ O ₄			35.1	64	0.251	
Microwave –initiated catalytic process	Ni _{1.25} Co _{0.5}	HDPE	–	50.2	77.7	0.181	[71]
Two –stage thermal catalytic process	FeNi1	PP	800	25.1	53.3	0.039	[72]
	FeNi2			20	46.7	0.031	
Two –stage thermal catalytic process	Fe-SiO ₂ -S	PP	800	15.4	41.7	0.024	[73]
	Fe-SiO ₂ -L			25.6	50.3	0.04	
Two –stage thermal catalytic process	La _{0.8} Ni _{0.15} Fe _{0.85} O _{3–δ}	LDPE	800	24.5	74.8	0.038	[74]
		HDPE		23.2	72.6	0.036	
Two –stage thermal catalytic process	La _{0.8} Ni _{0.15} Co _{0.5} O _{3–δ}	PP	800	19.8	–	0.031	[75]
Two –stage thermal catalytic process	Ni/γ- Al ₂ O ₃	Mixture of HDPE, LDPE,	800	31.8	62.9	0.05	[41]
	Fe/γ- Al ₂ O ₃	PP and PS		15.4	41.7	0.024	
	Ni-Fe/γ- Al ₂ O ₃			25.6	50.39	0.04	

study also supports the potential for USS-based catalysts in sustainable plastic waste recycling, reinforcing its viability for industrial applications. These findings contribute to advancing greener catalyst synthesis methods and improving the sustainability of waste-to-energy conversion processes.

3.7. Comparison of H₂ yield, selectivity and energy yield (gH₂/kWh) with representative literature

The H₂ yield and selectivity achieved in this study through plasma-thermal catalytic pyrolysis of plastic waste were benchmarked with representative literature studies, as summarized in Table 1. Notably, the plasma-alone process produced H₂ yields comparable to or even higher than those achieved with two-stage thermal catalytic pyrolysis. The developed plasma-thermal catalytic tandem process, utilizing La_{0.6}Ca_{0.4}Co_{0.2}Fe_{0.8}O_{3–δ} synthesized via ultrasonic spray synthesis, exhibited high H₂ yield and selectivity across all referenced studies, establishing it as a promising and efficient approach for converting waste plastics into hydrogen and carbon nanomaterials.

The energy yield of H₂ (gH₂/kWh) is an important parameter for assessing the economic viability of the process, as it directly quantifies the grams of H₂ produced per kWh of energy input. Since this metric is highly influenced by factors such as operating conditions, reactor size, feedstock type, and feedstock quantity, directly applying literature data for H₂ energy yield calculations may lead to misleading conclusions. To ensure a fair comparison, we incorporated several reasonable assumptions based on literature sources to account for variations in equipment parameters, operating conditions, and feedstock mass across different studies. A detailed analysis of energy consumption calculations and the corresponding H₂ energy yields for various studies is provided in Tables S9 and S10.

Our analysis demonstrates that the plasma-alone process achieves higher H₂ energy yields than most reported studies, primarily due to its high efficiency and short reaction time. However, while the plasma-thermal catalytic process initially shows a lower energy yield per batch, its performance improves significantly with successive cycles of operation. As shown in Table S10, the energy yield of H₂ (gH₂/kWh) increases with repeated cycles, whereas in microwave-assisted processes, it follows the opposite trend, decreasing with successive cycles.

This highlights the scalability potential of the plasma-thermal catalytic process for continuous hydrogen production. Further optimization of operational parameters, reactor design, and low-cost catalysts will be essential for enhancing overall process efficiency in the future.

4. Conclusions

This study introduces a novel plasma-thermal catalytic tandem process for the efficient decomposition of real-world plastic waste, enabling the simultaneous production of hydrogen-rich gases and high-value carbon nanomaterials. By integrating plasma technology with a thermal catalytic system, this approach significantly enhances hydrogen yield and selectivity while reducing liquid byproduct formation compared to conventional thermal catalytic methods. A comprehensive evaluation of perovskite-type LCCF pre-catalysts identified LCCF6428-USS as the best suitable formulation, achieving an H₂ yield of 54.7 mmol/g_{plastic} with a selectivity of 73.8 %. This enhancement is attributed to the plasma-induced chemical pathways, where highly energetic electrons and reactive species promote efficient decomposition beyond traditional thermal mechanisms. Furthermore, the plasma-thermal catalytic process facilitates the formation of carbon nanotubes due to Fe and Co species exsolution from the perovskite, which acts as active sites for nanoparticle growth. Life cycle assessment results indicate that ultrasonic spray synthesis is the more environmentally sustainable method than CP for LCCF production, offering lower energy consumption, reduced direct emissions, and decreased water usage across both small and large laboratory scales. Given the high catalytic performance and lower environmental impact of LCCF6428-USS among the investigated pre-catalysts, the plasma-enabled catalytic pyrolysis process using LCCF6428-USS presents a promising and sustainable strategy for plastic waste upcycling. To further improve the scalability and industrial applicability of this process, optimization of operational parameters such as nitrogen flow rate and plasma power is recommended. Additionally, integrating an automated plastic feeding system could enable continuous processing, facilitating large-scale deployment. Overall, this work presents an environmentally sustainable solution for plastic waste management, contributing to the advancement of circular economy initiatives.

CRediT authorship contribution statement

Xiao Yu: Writing – original draft, Validation, Methodology, Formal analysis, Data curation, Conceptualization. **Aasir Rashid:** Writing – review & editing, Validation, Methodology, Investigation. **Guoxing Chen:** Writing – review & editing, Validation, Supervision, Methodology, Funding acquisition, Formal analysis, Data curation, Conceptualization. **Marc Widenmeyer:** Writing – review & editing, Validation, Methodology. **Ulrike Kunz:** Resources, Investigation. **Tao Shao:** Writing – review & editing, Validation, Investigation. **Gert Homm:** Writing – review & editing, Funding acquisition. **Leopoldo Molina-Luna:** Writing – review & editing, Investigation. **Rony Snyders:** Writing – review & editing, Validation. **Anke Weidenkaff:** Writing – review & editing, Supervision, Funding acquisition.

Declaration of competing interest

The authors declare that they have no known competing financial interests or personal relationships that could have appeared to influence the work reported in this paper.

Acknowledgments

The authors are thankful to Jürgen Dieter Rossa for the kind support during the SEM-EDXS measurements. G.C. kindly thanks CHN Energy Europe Research GmbH for financial support during the Plasma-blade industrial project. R.S. thanks the EOS project PLASynth2 (application N 40007511) funded by the FWO and F.R.S.-FNRS under the Excellence of Science (EOS) program for financial support.

Appendix A. Supplementary material

Supplementary data to this article can be found online at <https://doi.org/10.1016/j.cej.2025.161954>.

Data availability

Data will be made available on request.

References

- [1] Plastics Europe, Plastics – the fast Facts 2023 • Plastics Europe, 2023, <https://plasticseurope.org/knowledge-hub/plastics-the-fast-facts-2023/>, accessed 8 March 2024.
- [2] J. Hopewell, R. Dvorak, E. Kosior, Plastics recycling: challenges and opportunities, *Philosop. Trans. Royal Soc. London Series B, Biol. Sci.* 364 (2009) 2115–2126, <https://doi.org/10.1098/rstb.2008.0311>.
- [3] S. King, S. Hutchinson, N. Boxall, *Advanced recycling technologies to address Australia's plastic waste*, CSIRO, 2021.
- [4] D. Cudjoe, H. Wang, Plasma gasification versus incineration of plastic waste: energy, economic and environmental analysis, *Fuel Process. Technol.* 237 (2022) 107470, <https://doi.org/10.1016/j.fuproc.2022.107470>.
- [5] J. Jiang, K. Shi, X. Zhang, K. Yu, H. Zhang, J. He, Y. Ju, J. Liu, From plastic waste to wealth using chemical recycling: a review, *J. Environ. Chem. Eng.* 10 (2022) 106867, <https://doi.org/10.1016/j.jece.2021.106867>.
- [6] V.K. Soni, G. Singh, B.K. Vijayan, A. Chopra, G.S. Kapur, S.S.V. Ramakumar, Thermochemical recycling of waste plastics by pyrolysis: a review, *Energy Fuels* 35 (2021) 12763–12808, <https://doi.org/10.1021/acs.energyfuels.1c01292>.
- [7] M. Solis, S. Silveira, Technologies for chemical recycling of household plastics - a technical review and TRL assessment, *Waste Manag.* 105 (2020) 128–138, <https://doi.org/10.1016/j.wasman.2020.01.038>.
- [8] M. Rajasekhar, N.V. Rao, G.C. Rao, G. Priyadarshini, N.J. Kumar, Energy generation from municipal solid waste by innovative technologies – plasma gasification, *Procedia Mater. Sci.* 10 (2015) 513–518, <https://doi.org/10.1016/j.mspro.2015.06.094>.
- [9] R. Mishra, C.-M. Shu, A.R. Gollakota, S.-Y. Pan, Unveiling the potential of pyrolysis-gasification for hydrogen-rich syngas production from biomass and plastic waste, *Energ. Convers. Manage.* 321 (2024) 118997, <https://doi.org/10.1016/j.enconman.2024.118997>.
- [10] W. Ma, C. Chu, P. Wang, Z. Guo, B. Liu, G. Chen, Characterization of tar evolution during DC thermal plasma steam gasification from biomass and plastic mixtures: parametric optimization via response surface methodology, *Energ. Convers. Manage.* 225 (2020) 113407, <https://doi.org/10.1016/j.enconman.2020.113407>.
- [11] L. Mazzoni, I. Janajreh, Plasma gasification of municipal solid waste with variable content of plastic solid waste for enhanced energy recovery, *Int. J. Hydrogen Energy* 42 (2017) 19446–19457, <https://doi.org/10.1016/j.ijhydene.2017.06.069>.
- [12] M.T. Munir, I. Mardon, S. Al-Zuhair, A. Shawabkeh, N.U. Saqib, Plasma gasification of municipal solid waste for waste-to-value processing, *Renew. Sustain. Energy Rev.* 116 (2019) 109461, <https://doi.org/10.1016/j.rser.2019.109461>.
- [13] S. King, K.E. Locock, A circular economy framework for plastics: a semi-systematic review, *J. Clean. Prod.* 364 (2022) 132503, <https://doi.org/10.1016/j.jclepro.2022.132503>.
- [14] B. Kunwar, H.N. Cheng, S.R. Chandrashekar, B.K. Sharma, Plastics to fuel: a review, *Renew. Sustain. Energy Rev.* 54 (2016) 421–428, <https://doi.org/10.1016/j.rser.2015.10.015>.
- [15] W. Gao, Y. Chang, Q. Zhou, Q. Wang, K.H. Lim, D. Wang, J. Hu, W.-J. Wang, B.-G. Li, P. Liu, Chemical recycling of polyolefin waste: from the perspective of efficient pyrolysis reactors, *Front. Chem. Sci. Eng.* 18 (2024) 1–25, <https://doi.org/10.1007/s11705-024-2498-x>.
- [16] H. Lin, L. Zhu, Y. Liu, V.S. Vladimirovich, B. Oboirien, Y. Zhou, Plastic upgrading via catalytic pyrolysis with combined metal-modified gallium-based HZSM-5 and MCM-41, *Front. Chem. Sci. Eng.* 18 (2024) 1–13, <https://doi.org/10.1007/s11705-024-2476-3>.
- [17] H. Kim, E. Nam, K. An, H. Lim, Laboratory-scale plastic upcycling and green growth: Evaluating the upcycling of plastic waste into carbon nanotubes from economic and environmental aspects, *Chem. Eng. J.* 495 (2024) 153300, <https://doi.org/10.1016/j.cej.2024.153300>.
- [18] F. Zhang, F. Wang, X. Wei, Y. Yang, S. Xu, D. Deng, Y.Z. Wang, From trash to treasure: Chemical recycling and upcycling of commodity plastic waste to fuels, high-valued chemicals and advanced materials, *J. Energy Chem.* 69 (2022) 369–388, <https://doi.org/10.1016/j.jechem.2021.12.052>.
- [19] P. Das, P. Tiwari, The effect of slow pyrolysis on the conversion of packaging waste plastics (PE and PP) into fuel, *Waste Manag.* 79 (2018) 615–624, <https://doi.org/10.1016/j.wasman.2018.08.021>.
- [20] D. Yao, H. Yang, H. Chen, P.T. Williams, Investigation of nickel-impregnated zeolite catalysts for hydrogen/syngas production from the catalytic reforming of waste polyethylene, *Appl. Catal. B* 227 (2018) 477–487, <https://doi.org/10.1016/j.apcatb.2018.01.050>.
- [21] R.K. Singh, B. Ruj, Time and temperature depended fuel gas generation from pyrolysis of real world municipal plastic waste, *Fuel* 174 (2016) 164–171, <https://doi.org/10.1016/j.fuel.2016.01.049>.
- [22] A. Veksha, A. Giannis, V.-W.-C. Chang, Conversion of non-condensable pyrolysis gases from plastics into carbon nanomaterials: effects of feedstock and temperature, *J. Anal. Appl. Pyrol.* 124 (2017) 16–24, <https://doi.org/10.1016/j.jaap.2017.03.005>.
- [23] X. Yu, G. Chen, M. Widenmeyer, I. Kinski, X. Liu, U. Kunz, D. Schüpfer, L. Molina-Luna, X. Tu, G. Homm, A. Weidenkaff, Catalytic recycling of medical plastic wastes over La_{0.6}Ca_{0.4}Co_{1-x}Fe_xO_{3-δ} pre-catalysts for co-production of H₂ and high-value added carbon nanomaterials, *Appl. Catal. B: Environ.* 334 (2023) 122838, <https://doi.org/10.1016/j.apcatb.2023.122838>.
- [24] I. Aminu, M.A. Nahil, P.T. Williams, Hydrogen from waste plastics by two-stage pyrolysis/low-temperature plasma catalytic processing, *Energy Fuels* 34 (2020) 11679–11689, <https://doi.org/10.1021/acs.energyfuels.0c02043>.
- [25] I. Aminu, M.A. Nahil, P.T. Williams, Pyrolysis-plasma/catalytic reforming of post-consumer waste plastics for hydrogen production, *Catal. Today* 420 (2023) 114084, <https://doi.org/10.1016/j.cattod.2023.114084>.
- [26] X. Jie, W. Li, D. Slocombe, Y. Gao, I. Banerjee, S. Gonzalez-Cortes, B. Yao, H. AlMegren, S. Alshihri, J. Dilworth, J. Thomas, T. Xiao, P. Edwards, Microwave-initiated catalytic deconstruction of plastic waste into hydrogen and high-value carbons, *Nat. Catal.* 3 (2020) 902–912, <https://doi.org/10.1038/s41929-020-00518-5>.
- [27] W. Chen, Y. Zhou, Y. Wang, Y. Zhong, Y. Yu, K. Huang, Microwave-assisted pyrolysis of plastic waste with magnetic catalysts in a multi-ridge field compressed reactor, *J. Anal. Appl. Pyrol.* 179 (2024) 106440, <https://doi.org/10.1016/j.jaap.2024.106440>.
- [28] J. Zhao, J. Gao, D. Wang, Y. Chen, L. Zhang, W. Ma, S. Zhao, Microwave-intensified catalytic upcycling of plastic waste into hydrogen and carbon nanotubes over self-dispersing bimetallic catalysts, *Chem. Eng. J.* 483 (2024) 149270, <https://doi.org/10.1016/j.cej.2024.149270>.
- [29] H. Wang, B. Zhang, P. Luo, K. Huang, Y. Zhou, Simultaneous achievement of high-yield hydrogen and high-performance microwave absorption materials from microwave catalytic deconstruction of plastic waste, *Processes* 10 (2022) 782, <https://doi.org/10.3390/pr10040782>.
- [30] B. Zhang, H. Wang, Y. Yang, Y. Zhou, B. Zhang, K. Huang, Microwave-carbon fiber cloth co-ignited catalytic degradation of waste plastic into high-yield hydrogen and carbon nanotubes, *J. Environ. Chem. Eng.* 11 (2023) 109710, <https://doi.org/10.1016/j.jece.2023.109710>.
- [31] X. Yu, Z. Rao, G. Chen, Y. Yang, S. Yoon, L. Liu, Z. Huang, M. Widenmeyer, H. Guo, G. Homm, U. Kunz, X. Liu, E. Ionescu, L. Molina-Luna, X. Tu, Y. Zhou, A. Weidenkaff, Plasma-enabled process with single-atom catalysts for sustainable plastic waste transformation, *Angew. Chem. Int. Ed.* 63 (2024) e202404196, <https://doi.org/10.1002/anie.202404196>.
- [32] C. Yuwen, B. Liu, Q. Rong, K. Hou, L. Zhang, S. Guo, Enhanced microwave absorption capacity of iron-based catalysts by introducing Co and Ni for microwave pyrolysis of waste COVID-19 Masks, *Fuel* 340 (2023) 127551, <https://doi.org/10.1016/j.fuel.2023.127551>.
- [33] L. Yao, B. Yi, X. Zhao, W. Wang, Y. Mao, J. Sun, Z. Song, Microwave-assisted decomposition of waste plastic over Fe/FeAl₂O₄ to produce hydrogen and carbon

- nanotubes, *J. Anal. Appl. Pyrol.* 165 (2022) 105577, <https://doi.org/10.1016/j.jaap.2022.105577>.
- [34] A. Weidenkaff, S.G. Ebbinghaus, T. Lippert, $\text{Ln}_{1-x}\text{A}_x\text{CoO}_3$ (Ln = Er, La; A = Ca, Sr)/carbon nanotube composite materials applied for rechargeable Zn/Air batteries, *Chem. Mater.* 14 (2002) 1797–1805, <https://doi.org/10.1021/cm011305v>.
- [35] G. Ren, Z. Luo, Y. Duan, X. Liu, Z. Yuan, F. Cai, Carbon nanotube@ Mn_3O_4 composite as cathode for high-performance aqueous zinc ion battery, *J. Alloy. Compd.* 898 (2022) 162747, <https://doi.org/10.1016/j.jallcom.2021.162747>.
- [36] A. Weidenkaff, S.G. Ebbinghaus, T. Lippert, M.J. Montenegro, C. Soltmann, R. Wessicken, Phase formation and phase transition of $\text{Ln}_{1-x}\text{Ca}_x\text{CoO}_3$ (Ln = La, Er) applied for bifunctional air electrodes, *Cryst. Eng.* 5 (2002) 449–457, [https://doi.org/10.1016/S1463-0184\(02\)00056-4](https://doi.org/10.1016/S1463-0184(02)00056-4).
- [37] D.-M. Amaya-Dueñas, G. Chen, A. Weidenkaff, N. Sata, F. Han, I. Biswas, R. Costa, K.A. Friedrich, A-site deficient chromite with in situ Ni exsolution as a fuel electrode for solid oxide cells (SOCs), *J. Mater. Chem. A* 9 (2021) 5685–5701, <https://doi.org/10.1039/D0TA07090D>.
- [38] G. Chen, W. Liu, M. Widenmeyer, P. Ying, M. Dou, W. Xie, C. Bubeck, L. Wang, M. Fyta, A. Feldhoff, A. Weidenkaff, High flux and CO_2 -resistance of $\text{La}_{0.6}\text{Ca}_{0.4}\text{Co}_{1-x}\text{Fe}_x\text{O}_{3-\delta}$ oxygen-transporting membranes, *J. Memb. Sci.* 590 (2019) 117082, <https://doi.org/10.1016/j.memsci.2019.05.007>.
- [39] A. Rashid, H. Lim, D. Plaz, G. Escobar Cano, M. Bresser, K.-S. Wiegiers, G. Confalonieri, S. Baek, G. Chen, A. Feldhoff, A. Schulz, A. Weidenkaff, M. Widenmeyer, Hydrogen-tolerant $\text{La}_{0.6}\text{Ca}_{0.4}\text{Co}_{0.2}\text{Fe}_{0.8}\text{O}_{3-\delta}$ oxygen transport membranes from ultrasonic spray synthesis for plasma-assisted CO_2 conversion, *Membranes* 13 (2023) 875, <https://doi.org/10.3390/membranes13110875>.
- [40] G. Chen, W. Liu, M. Widenmeyer, X. Yu, Z. Zhao, S. Yoon, R. Yan, W. Xie, A. Feldhoff, G. Homm, E. Ionescu, M. Fyta, A. Weidenkaff, Advancing oxygen separation: insights from experimental and computational analysis of $\text{La}_{0.3}\text{Ca}_{0.3}\text{Co}_{0.3}\text{Fe}_{0.6}\text{M}_{0.1}\text{O}_{3-\delta}$ (M = Cu, Zn) oxygen transport membranes, *Front. Chem. Sci. Eng.* 18 (2024) 1–13, <https://doi.org/10.1007/s11705-024-2421-5>.
- [41] D. Yao, Y. Zhang, P.T. Williams, H. Yang, H. Chen, Co-production of hydrogen and carbon nanotubes from real-world waste plastics: influence of catalyst composition and operational parameters, *Appl. Catal. B* 221 (2018) 584–597, <https://doi.org/10.1016/j.apcatb.2017.09.035>.
- [42] D. Yao, C. Wu, H. Yang, Y. Zhang, M.A. Nahil, Y. Chen, P.T. Williams, H. Chen, Co-production of hydrogen and carbon nanotubes from catalytic pyrolysis of waste plastics on Ni-Fe bimetallic catalyst, *Energ. Convers. Manage.* 148 (2017) 692–700, <https://doi.org/10.1016/j.enconman.2017.06.012>.
- [43] Y. Shen, W. Gong, B. Zheng, L. Gao, Ni–Al bimetallic catalysts for preparation of multiwalled carbon nanotubes from polypropylene: Influence of the ratio of Ni/Al, *Appl. Catal. B* 181 (2016) 769–778, <https://doi.org/10.1016/j.apcatb.2015.08.051>.
- [44] S. Wang, Y. Zhang, R. Shan, J. Gu, T. Huhe, X. Ling, H. Yuan, Y. Chen, High-yield H_2 production from polypropylene through pyrolysis-catalytic reforming over activated carbon based nickel catalyst, *J. Clean. Prod.* 352 (2022) 131566, <https://doi.org/10.1016/j.jclepro.2022.131566>.
- [45] Y. Zhu, J. Miao, Y. Zhang, C. Li, Y. Wang, Y. Cheng, M. Long, J. Wang, C. Wu, Carbon nanotubes production from real-world waste plastics and the pyrolysis behaviour, *Waste Manag.* 166 (2023) 141–151, <https://doi.org/10.1016/j.wasman.2023.05.002>.
- [46] N. Cai, X. Li, S. Xia, L. Sun, J. Hu, P. Bartocci, F. Fantozzi, P.T. Williams, H. Yang, H. Chen, Pyrolysis-catalysis of different waste plastics over Fe/ Al_2O_3 catalyst: High-value hydrogen, liquid fuels, carbon nanotubes and possible reaction mechanisms, *Energ. Convers. Manage.* 229 (2021) 113794, <https://doi.org/10.1016/j.enconman.2020.113794>.
- [47] N. Cai, S. Xia, X. Li, H. Xiao, X. Chen, Y. Chen, P. Bartocci, H. Chen, P.T. Williams, H. Yang, High-value products from ex-situ catalytic pyrolysis of polypropylene waste using iron-based catalysts: the influence of support materials, *Waste Manag.* 136 (2021) 47–56, <https://doi.org/10.1016/j.wasman.2021.09.030>.
- [48] Q. Cao, H.-C. Dai, J.-H. He, C.-L. Wang, C. Zhou, X.-F. Cheng, J.-M. Lu, Microwave-initiated $\text{MAX Ti}_3\text{AlC}_2$ -catalyzed upcycling of polyolefin plastic wastes: selective conversion to hydrogen and carbon nanofibers for sodium-ion battery, *Appl. Catal. B* 318 (2022) 121828, <https://doi.org/10.1016/j.apcatb.2022.121828>.
- [49] K.R. Parmar, V. Tuli, A. Caiola, J. Hu, Y. Wang, Sustainable production of hydrogen and carbon nanotubes/nanofibers from plastic waste through microwave degradation, *Int. J. Hydrogen Energy* 51 (2024) 488–498, <https://doi.org/10.1016/j.ijhydene.2023.08.224>.
- [50] X. Liu, D. Xu, H. Ding, M. Widenmeyer, W. Xie, M. Mellin, F. Qu, G. Chen, Y. S. Zhang, Z. Zhang, A. Rashid, L. Molina-Luna, J.P. Hofmann, R. Riedel, D.J. Brett, A. Weidenkaff, Multi-scale designed $\text{Co}_x\text{Mn}_{3-x}\text{O}_4$ spinels: Smart pre-catalysts towards high-efficiency pyrolysis-catalysis recycling of waste plastics, *Appl. Catal. B* 324 (2023) 122271, <https://doi.org/10.1016/j.apcatb.2022.122271>.
- [51] C. Wu, M.A. Nahil, N. Miskolczi, J. Huang, P.T. Williams, Production and application of carbon nanotubes, as a co-product of hydrogen from the pyrolysis-catalytic reforming of waste plastic, *Process Saf. Environ. Prot.* 103 (2016) 107–114, <https://doi.org/10.1016/j.psep.2016.07.001>.
- [52] Q.-L. Li, R. Shan, S.-X. Wang, H.-R. Yuan, Y. Chen, Production of carbon nanotubes via catalytic pyrolysis of waste plastics over Ni/ Al_2O_3 catalyst: the influence of plastic types, *J. Anal. Appl. Pyrol.* 177 (2024) 106318, <https://doi.org/10.1016/j.jaap.2023.106318>.
- [53] din-de, Umweltmanagement - Ökobilanz - Grundsätze und Rahmenbedingungen (ISO 14040:2006 + Amd 1:2020); Deutsche Fassung EN ISO 14040:2006 + A1: 2020, 2024, <https://www.din.de/de/forschung-und-innovation/themen/wasserstoff/normensuche/norm-einzelsicht/din-en-iso-14040-964864>, accessed 30 July 2024.
- [54] din-de, Umweltmanagement - Ökobilanz - Anforderungen und Anleitungen (ISO 14044:2006 + Amd 1:2017 + Amd 2:2020); Deutsche Fassung EN ISO 14044:2006 + A1:2018 + A2:2020, 2024, <https://www.din.de/de/forschung-und-innovation/themen/wasserstoff/normensuche/norm-einzelsicht/din-en-iso-14044-963856>, accessed 30 July 2024.
- [55] S. Sala, technical note for CFs - ILCD LCIA.
- [56] J. Fu, N.N. Daanen, E.E. Rugen, D.P. Chen, S.E. Skrabalak, Simple reactor for ultrasonic spray synthesis of nanostructured materials, *Chem. Mater.* 29 (2017) 62–68, <https://doi.org/10.1021/acs.chemmater.6b02660>.
- [57] Internal Market, Industry, Entrepreneurship and SMEs, Critical raw materials, 2024, https://single-market-economy.ec.europa.eu/sectors/raw-materials/areas-specific-interest/critical-raw-materials_en#fifth-list-2023-of-critical-raw-materials-for-the-eu, accessed 23 October 2024.
- [58] G. Kou, L. Guo, H. Li, N. Liu, W. Li, H. Shen, L. Bai, Synchronous growth of bamboo-shaped CNTs and PyC for fabricating super-elastic nanocomposites, *Compos. B Eng.* 174 (2019) 107029, <https://doi.org/10.1016/j.compositesb.2019.107029>.
- [59] C.N. He, N.Q. Zhao, X.W. Du, C.S. Shi, J.J. Li, F. He, Characterization of bamboo-shaped CNTs prepared using deposition-precipitation catalyst, *Mater. Sci. Eng. A* 479 (2008) 248–252, <https://doi.org/10.1016/j.msea.2007.06.048>.
- [60] R. Garg, K. Kaur, U.K. Gautam, Mapping the scalability, effect of reaction atmosphere, and catalyst dose in bamboo-like CNT synthesis for efficient electrocatalysis, *Int. J. Hydrogen Energy* 61 (2024) 914–921, <https://doi.org/10.1016/j.ijhydene.2024.02.274>.
- [61] M. Kumar, Y. Ando, Chemical vapor deposition of carbon nanotubes: a review on growth mechanism and mass production, *J. Nanosci. Nanotechnol.* 10 (2010) 3739–3758, <https://doi.org/10.1166/jnn.2010.2939>.
- [62] J.-P. Tessonnier, D.S. Su, Recent progress on the growth mechanism of carbon nanotubes: a review, *Chem. Sus. Chem.* 4 (2011) 824–847, <https://doi.org/10.1002/cssc.201100175>.
- [63] J.C. Acomb, C. Wu, P.T. Williams, The use of different metal catalysts for the simultaneous production of carbon nanotubes and hydrogen from pyrolysis of plastic feedstocks, *Appl. Catal. B* 180 (2016) 497–510, <https://doi.org/10.1016/j.apcatb.2015.06.054>.
- [64] R.-X. Yang, K.-H. Chuang, M.-Y. Wey, Effects of nickel species on Ni/ Al_2O_3 catalysts in carbon nanotube and hydrogen production by waste plastic gasification: bench- and pilot-scale tests, *Energy Fuels* 29 (2015) 8178–8187, <https://doi.org/10.1021/acs.energyfuels.5b01866>.
- [65] D. Yao, H. Yang, H. Chen, P.T. Williams, Co-precipitation, impregnation and so-gel preparation of Ni catalysts for pyrolysis-catalytic steam reforming of waste plastics, *Appl. Catal. B* 239 (2018) 565–577, <https://doi.org/10.1016/j.apcatb.2018.07.075>.
- [66] F. Tuinstra, J. Koenig, Raman spectrum of graphite, *J. Chem. Phys.* (1970).
- [67] M.S. Dresselhaus, G. Dresselhaus, R. Saito, A. Jorio, Raman spectroscopy of carbon nanotubes, *Phys. Rep.* 409 (2005) 47–99, <https://doi.org/10.1016/j.physrep.2004.10.006>.
- [68] L.M. Malard, M.A. Pimenta, G. Dresselhaus, M.S. Dresselhaus, Raman spectroscopy in graphene, *Phys. Rep.* 473 (2009) 51–87, <https://doi.org/10.1016/j.physrep.2009.02.003>.
- [69] S.D.M. Brown, A. Jorio, M.S. Dresselhaus, G. Dresselhaus, Observations of the D-band feature in the Raman spectra of carbon nanotubes, *Phys. Rev. B* 64 (2001) 73403, <https://doi.org/10.1103/PhysRevB.64.073403>.
- [70] Y. Wang, T. Biddle, C. Jiang, T. Luong, R. Chen, S. Brown, X. Jie, J. Hu, Microwave-driven upcycling of single-use plastics using zeolite catalyst, *Chem. Eng. J.* 465 (2023) 142918, <https://doi.org/10.1016/j.cej.2023.142918>.
- [71] J. Wang, Y. Pan, J. Song, Q. Huang, A high-quality hydrogen production strategy from waste plastics through microwave-assisted reactions with heterogeneous bimetallic iron/nickel/ cerium catalysts, *J. Anal. Appl. Pyrol.* 166 (2022) 105612, <https://doi.org/10.1016/j.jaap.2022.105612>.
- [72] D. Yao, H. Li, Y. Dai, C.-H. Wang, Impact of temperature on the activity of Fe-Ni catalysts for pyrolysis and decomposition processing of plastic waste, *Chem. Eng. J.* 408 (2021) 127268, <https://doi.org/10.1016/j.cej.2020.127268>.
- [73] X. Liu, Y. Zhang, M.A. Nahil, P.T. Williams, C. Wu, Development of Ni- and Fe-based catalysts with different metal particle sizes for the production of carbon nanotubes and hydrogen from thermo-chemical conversion of waste plastics, *J. Anal. Appl. Pyrol.* 125 (2017) 32–39, <https://doi.org/10.1016/j.jaap.2017.05.001>.
- [74] J. Jia, A. Veksha, T.-T. Lim, G. Lisak, Weakening the strong Fe-La interaction in A-site-deficient perovskite via Ni substitution to promote the thermocatalytic synthesis of carbon nanotubes from plastics, *J. Hazard. Mater.* 403 (2021) 123642, <https://doi.org/10.1016/j.jhazmat.2020.123642>.
- [75] J. Jia, A. Veksha, T.-T. Lim, G. Lisak, Temperature-dependent synthesis of multi-walled carbon nanotubes and hydrogen from plastic waste over A-site-deficient perovskite $\text{La}_{0.8}\text{Ni}_{1-x}\text{Co}_x\text{O}_{3-\delta}$, *Chemosphere* 291 (2022) 132831, <https://doi.org/10.1016/j.chemosphere.2021.132831>.